GEORG-AUGUST-UNIVERSITÄT
GÖTTINGEN

Fakultät für
Physik

Bachelor's Thesis

Untersuchung von Modellierungsunsicherheiten in $t\bar{t}$-Paarproduktion am ATLAS-Experiment

Study of modelling uncertainties in $t\bar{t}$ pair production at the ATLAS experiment

prepared by

Jun Huang

from Wuhan

at the II. Physikalisches Institut

Thesis number: II.Physik-UniGö-BSc-2020/03

Thesis period: 1st April 2020 until 6th July 2014

First referee: Prof. Dr. Arnulf Quadt

Second referee: Prof. Dr. Ariane Frey

Contents

1 Introduction **1**

2 Theoretical Background **2**

2.1 Standard Model 2

2.2 The Top Quark 3

2.2.1 Top Quarks at the LHC 3

3 Experimental Setup **6**

3.1 Detector 6

3.2 ATLAS 6

3.3 ALTAS detector 7

3.3.1 Inner Detector 8

3.3.2 Calorimeter 9

3.3.3 Muon Detector 9

3.3.4 Data processing analysis system 9

4 Introduction to top quark analysis **11**

4.1 Monte Carlo simulation 11

4.2 Monte Carlo samples 12

5 Comparison between the FSR and ISR uncertainties estimation in old and new approach **14**

5.1 Comparison between up and down impact of each variation in ISR and FSR 14

5.1.1 Explanation 14

5.1.2 H_T and N_{jets} multiplicity distributions for individual variations of both ISR and FSR for single electron 15

5.1.3 H_T and N_{jets} multiplicity distributions for individual variations of both ISR and FSR for single muon 20

5.1.4 Discussion 25

5.2 Comparison of histogram total uncertainty and ratio total uncertainty between 4 variations . . . 26
5.2.1 Comparing and Discussion . . . 26
5.3 Comparison of nominal histograms with modified error in the new approach 26
5.3.1 Explanation . . . 27
5.3.2 Comparison of variations contributions to the uncertainty on nominal histograms in lepton+jets event . . . 27
5.3.3 Discussion . . . 37
5.4 Comparison of ISR/FSR uncertainties in the new/old approach with the largest impact variation . . . 37
5.4.1 Explanation . . . 37
5.4.2 Comparison of ISR/FSR uncertainties in the new/old approach with largest impacted variation in e+jet event . . . 38
5.4.3 Comparison of ISR/FSR uncertainties in the new/old approach with largest impacted variation in μ+jet event . . . 42
5.4.4 Discussion . . . 46

6 Conclusion and outlook **51**
6.1 Summary . . . 51
6.1.1 On total uncertainty level . . . 51
6.1.2 On 4 variations level . . . 51
6.1.3 On "up" and "down" variation level . . . 52
6.2 Outlook . . . 53

1 Introduction

About 2,500 years ago, Greek philosophers believed that after being divided innumerable times, matter would eventually become too small to be indivisible. The word atom is derived from Greek and means "indivisible".

In 1897, the first subatomic particle, the electron, was discovered by J.J Thomson. In 1911, Rutherford discovered that each atom contained a positively charged nucleus, and later in 1919 he discovered positively charged protons inside the nucleus. In 1932, uncharged neutrons were discovered by Chadwick. Prior to the 1950s, it was generally believed that atoms were composed of electrons, protons and neutrons, and these were considered the most basic units of matter.

With the development of particle accelerators and particle detectors, scientists have discovered that neutrons and protons are one type of hadrons, composed of smaller quark particles. The Standard Model of particle physics was developed in parallel to theoretically describe the interaction between elementary particles at the subatomic level.

To examine the theory both physical experiment and computer simulation are made. This thesis will mainly focus on the uncertainty in the computer simulation.

2 Theoretical Background

2.1 Standard Model

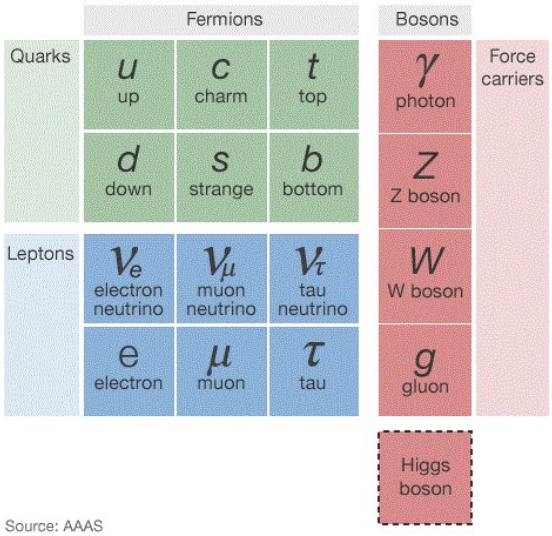

Figure 2.1: Particles of the Standard Model ©AAAS.

The Standard Model (SM) is the best known theory describing three basic forces: strong, weak, and electromagnetic forces, and the fundamental particles that make up all matter. It uses the Yang-Mills equation as its core and is also known as canonical symmetry field theory. This theory has dominated the development of physics since the 1950s and is highly consistent with experiments. The SM describes most experimental observations well but it is know, for example from neutrino oscillation or cosmological observations, that it is not complete.

The standard model contains fermions and bosons. Fermions are particles with half-integer spins and follow the Pauli exclusion principle; bosons have integer spins and do not follow the Pauli exclusion principle. In simple terms, fermions are particles that make up matter and bosons are responsible for transmitting various forces.

From Figure 2.1, we can see that fermions can be divided into quarks and leptons, of which quarks are divided into 6 quarks and into 3 generations: up and down quarks are the first generation, charm and strange quarks the second generation and the top and bottom quarks are the third generation. Up, charm and top quark have the charge of +2/3 e, and down, strange and bottom quark carry -1/3 e. Leptons are also divided in three generations: electrons, muon and tau with charge of -e and corresponding neutral neutrinos. There is also antiparticles of all the fermions which have opposite charges.

Bosons are the particles which mediate forces between the fermions. Photons mediate the electromagnetic force, gluons mediate the strong force, and Z bosons and W bosons mediate the weak force. The higgs mechanism describes how particles obtain there masses by interacting with a so-called higgs-field. A consequence if this field is a scalaer bosons, the higgs-boson, which was discovered in 2012 by the ATLAS and CMS experiments at the LHC.

2.2 The Top Quark

The top quark was discovered by the CDF and D0 experiments at Fermilab in 1995 [1][2] and is currently the heaviest known quark, its mass is $173.0 \pm 0.4\,\mathrm{GeV}$ [3]. Like other quarks, top quarks belong to fermions, have a spin of $\frac{1}{2}$, and have a charge of $+2/3$ e. The top quark interacts with other elementary particles through the strong force. The life time of the top quark is very short, only $5 \times 10^{-25}\,\mathrm{s}$. Before it has the time to form hadrons, it decays into a W boson and a bottom quark through the weak force.

2.2.1 Top Quarks at the LHC

Because the mass of the top quark is very large, according to Einstein's formula for mass and energy, we know that higher mass requires higher energy. Thus, top quarks could only be produced at the Tevatron and the LHC till now by pair production via the strong interaction or as single top quark via the weak interaction.

At the LHC top-quark pairs are usually produced by gluon fusion. Top quarks can also be produced via the weak interaction, which is related to W boson exchanges (s-channel, t-channel, Wt-channel).

Top quarks decay via the weak interaction, usually top quarks will decay into a W boson and a bottom quark, after that the W boson would rapidly decay into lepton and neutrino or quark and antiquark. When both W bosons decay into quarks, we could observe 6 jets ($b\bar{b}$ quarks and quarks from W boson decay); when both W bosons decay into leptons and neutrinos, we could observe 2 jets (b quarks) with 2 charged leptons; when only one of two W bosons decays into lepton and neutrino while the other one decays into quark and antiquark, we could observe 4 jets (b quarks and quark antiquark from W boson decay) and 1 charged lepton. The resulting decay modes are summarized in Table 2.1.

	jet	lepton	reaction
all jets	6	0	$t\bar{t} \to b\bar{b}W^+W^- \to b\bar{b}q_1\bar{q}_2q_3\bar{q}_4$
jets with lepton	4	1	$t\bar{t} \to b\bar{b}W^+W^- \to b\bar{b}q_1\bar{q}_2l\bar{\nu}_l$ / $b\bar{b}q_1\bar{q}_2\bar{l}\nu_l$
dilepton	2	2	$t\bar{t} \to b\bar{b}W^+W^- \to l_1\bar{\nu_{l_1}}\bar{l_2}\nu_{l_2}$

Table 2.1: Top quarks decays after pair production.

The predicted cross section of top quark pair production at the LHC at different energies is given in Table 2.2 :

energy	cross section
$\sqrt{s}$= 7 TeV	$\sigma_{t\bar{t}} = 177.3^{+4.6+9.0}_{-6.0-9.0}$ pb
$\sqrt{s}$= 8 TeV	$\sigma_{t\bar{t}} = 252.9^{+6.4+11.5}_{-8.6-11.5}$ pb
$\sqrt{s}$= 13 TeV	$\sigma_{t\bar{t}} = 831.8^{+19.8+35.1}_{-29.2-35.1}$ pb
$\sqrt{s}$= 14 TeV	$\sigma_{t\bar{t}} = 984.5^{+23.2+41.3}_{-34.7-41.3}$ pb

Table 2.2: Cross section theoretical prediction for $t\bar{t}$ pair production at the LHC assuming a top-quark mass of 172.5 GeV/c^2 [4]

The measurement of the $t\bar{t}$ production cross-section in the lepton+jets channel at $\sqrt{s}$=13 TeV with the ATLAS experiment using a data sample of $\mathcal{L}$= 139 fb^{-1} yields $\sigma_{t\bar{t}} = 830 \pm 0.4(stat.)^{+38.2}_{-37.0}(syst.)$ pb [5].
The systematic uncertainties are summarized in Table 2.3 [5]:

Experimental uncertainties	luminosity, pile up, lepton identification, reconstruction, isolation and trigger, lepton momentum scale and resolution, jet energy scale, jet energy resolution, jet-vertex-tagger(JVT) efficiency, flavour tagging, missing transverse energy scale and resolution
Signal modelling	top quark p_T reweighting, scale uncertainties, parton distribution functions(PDFs), parton shower and hadronisation
Background modelling	multijet, single-top, W+jets, other background processes

Table 2.3: Uncertainties of the cross section in $t\bar{t}$ pair production at the LHC.

3 Experimental Setup

3.1 Detector

The 27 km long Large Hadron Collider (LHC) causes two beams of protons to collide. Each beam has an energy of 6.5 TeV. High-energy particles made by particle accelerators must be observed by particle detectors. In order to detect the phenomena produced, particle detector must be able to detect these particles and measure their mass, momentum, energy, charge, and spin. In order to identify each particle made by the collision at the interaction point, the particle detectors must usually be designed in different layers each dedicated for a specific purpose. Different types of detectors make up different detection layers, and each type of detector is specialized in detecting a specific type of particles. The information left by the particles in different detection layers can be used to confirm the identity of the particles and accurately measure their energy and momentum. The role of each detection layer in the detector will be discussed in Section 3.3. The size of detector is huge due to high resolution and multiplicity functions. At the LHC, ATLAS is the largest particle detector with other detectors such as CMS, Alice and LHCb. With their help, scientists successfully discovered the Higgs particle at the LHC in 2012.

3.2 ATLAS

The ATLAS (A Toroidal LHC ApparatuS) [6] detector is a multipurpose particle detector with a height of 25 m and a length of 44 m (see Figure 3.1). When a proton beam made by the Large Hadron Collider (LHC) performs scattering experiments at the centre of the detector, many kinds of particles with different energies are generated. The ATLAS detector is not focused on a specific physical process. It is designed to detect a wide range of possible signals. ALTAS measure the deposited energies and tracks of the decay products[1]. The unique challenges faced by the Large Hadron Collider unprecedented high energy and extremely high collision frequencies require ATLAS to be larger and more complex than previously built detectors.

[1]ATLAS can not measure neutrinos.

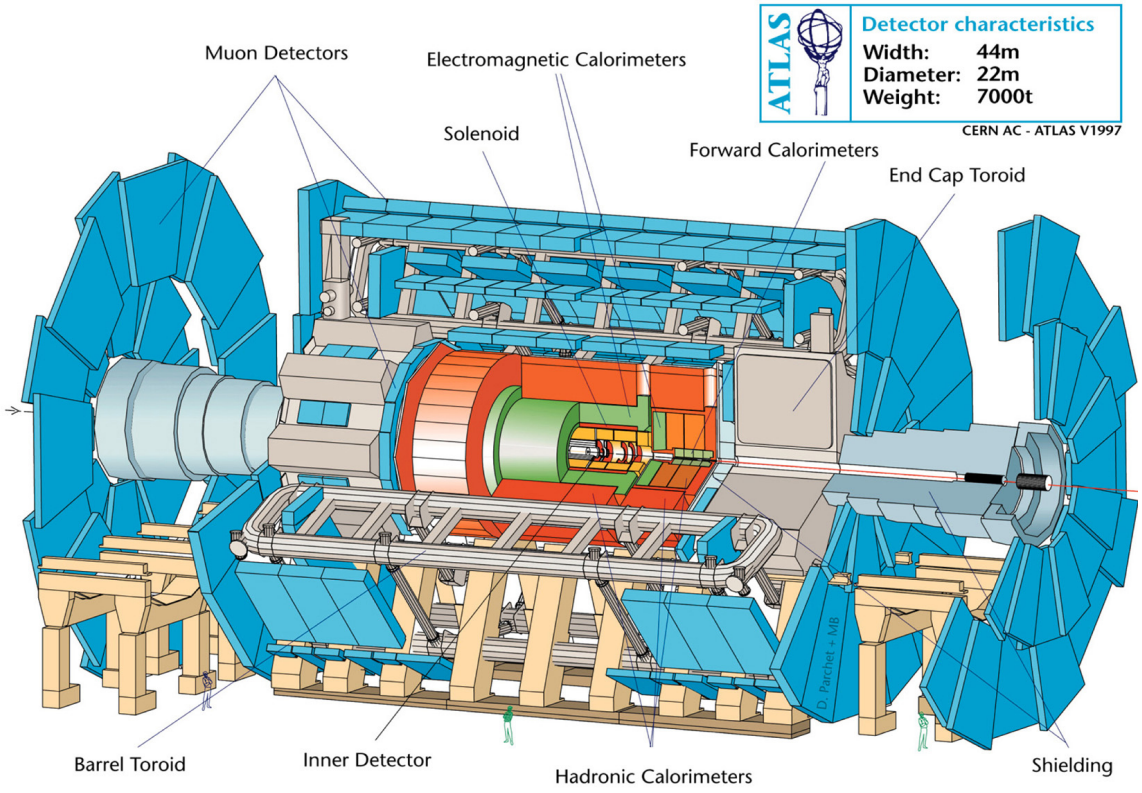

Figure 3.1: Cut-away view of the ATLAS detector ©CERN.

3.3 ALTAS detector

The ATLAS detector is composed of a series of concentric-axis cylindrical shell-type equipment and disk-type equipment at both ends of the centre, which is mainly divided into four parts: Inner detector, electromagnetic and hadronic calorimeter, and muon detector. Each of these sections is subdivided into several layers.

The functions of each detector are complementary: the inner detector accurately determines the trajectory of charged particles, the calorimeter measures the energy of those particles, and the muon subsystem provides additional measurement data for highly penetrating muons. The magnetic field generated by the magnet system causes charged particles to deflect as they move around the inner detector and muon chambers. The muon spectrometer can measure the momentum of these particles from the curvature of the deflection.

Neutrinos are the only known stable particles that cannot be detected directly; from the analysis of the momentum imbalance of the detected particles, the existence of neu-

trinos can be inferred. In order to achieve the above goals, the detector must be a 4π detector, i.e. all particles except neutrinos must be detected to avoid any detection blind spots.

3.3.1 Inner Detector

By detecting the interaction of scattered charged particles with materials at different positions, the movement of these particles can be tracked. Because the inner detector [6] is immersed in a 2 Tesla magnetic field, the charged particles moving in its space will be deflected, its direction shows the electrical properties of the charged particles, and its angle shows the momentum of the particles. The starting point of the trajectory can provide useful information for particle identification. For example, if the initial point of a series of particle trajectories is not the collision point of protons, this indicates that these particles originate from the decay of a bottom quark. The inner detector has three parts, which will be explained in detail below.

Pixel Detector

The pixel detector is the innermost part of the detector. Four precise positions can be given for each particle trajectory. The pixel detector has a total of more than 100 million data readout channels.

Semi Conductor Tracker

The Semiconductor Tracker (SCT) is the middle part of the inner detector. It can give at least four precise positions for each particle trajectory. In contrast to the pixel detector, the SCT uses silicon strips to measure particle trajectories.

Transition Radiation Tracker

The Transition Radiation Tracker (TRT) is the outermost part of the inner detector. It is a combination of a straw tracker and a transition radiation detector. Transitional radiation trackers have two main functions: Accurately track charged particles and correctly identify electrons. Each straw is filled with a Xenon gas mixture, and when the charged particles pass through, the gas mixture is ionised and the straw generates a current pulse (signal). By analysing the patterns formed by these pulsed wires, the trajectory of ion movement can be determined.

3.3.2 Calorimeter

The solenoid carrying the current is placed outside the inner detector, and the calorimeter [6] is located outside the solenoid. The purpose of the calorimeter is to measure the energy of the particles by absorbing them. There are two basic types of calorimetric systems: the Electromagnetic Calorimeter is the inner calorimeter and the Hadron Calorimeter is the outer one (see Figure 3.1). Both are sampling calorimeters.

In a sampling calorimeter, the material that absorbs the particle energy to generate a particle shower is different from the material that measures the shower energy and is separated in different areas.

Electromagnetic Calorimeter

An electromagnetic calorimeter absorbs energy from particles involved in electromagnetic interactions. This includes elecctrons and photons. The material used to absorb the energy to generate the particle shower is lead and stainless steel, and the material for the sampling layers is liquid Argon.

Hadron Calorimeter

Particles that do not loose a significant amount of enegry in the electromagnetic calorimter, mostly hadrons, will interact in the hadronic calorimeter. The Hadron calorimeter uses copper and tungsten as absorbers, the sampling material is steel.

3.3.3 Muon Detector

The muon spectrometer works similarly to the inner detector, the momentum of muons can be determined by the muon trajectory deflected by the magnetic field. This is important for the accurate measurement of the total momentum and analysis of neutrino-related data.

The muon spectrometer is used in the trigger system, which selects a pre-defined choice of events of interest which is motivated by physics arguments.

3.3.4 Data processing analysis system

Detectors can generate massive amounts of data that are difficult to store, the trigger system uses simple information to identify those interesting events in real time and retain

their information for detailed analysis. All events that are permanently stored will be reconstructed offline, which will regularly convert the signals obtained by the detector into physical objects, such as jets, photons and leptons.

4 Introduction to top quark analysis

At the LHC experiments, a lot of data is obtained by many different processes. Within the detectors, only the final state products, such as the final decay products of a top-quark, are observed. These have to be reconstructed to gain insight of the initial production process. In general, the following approach is being used: first use computer simulations to generate artificial events and then compare the measured events to the simulation to infer the process.

The analytical solution are unavailable to make predictions for the hard scattering process so numerical integration is required. However, Newton or Gaussian integration can only deal with a small number of final states, therefore numerical sampling of Monte Carlo events are used as experimental predictions based on the event probability distribution.

4.1 Monte Carlo simulation

Almost all analyses of the LHC are using event generators. In these predictions, a fixed-order of the matrix element is used, and a consistent matching or merging is performed between the matrix element and the parton shower contribution. The components of this prediction are based on approximations, so it is necessary to estimate their reliability, which is part of this thesis.

For a fixed order (matrix elements), the uncertainty estimate comes from changing the common factorisation (μ_F) and renormalisation (μ_R) scales, an additional uncertainty comes from the choice of the parton distribution function (PDF)[1]. Uncertainties in other parts of the prediction (such as parton showers, multi parton interactions and hadronisation) are difficult to estimate and require tuning of the used shower and hadronisation

[1]Parton distribution function (PDF) describes probability density for finding a particle with a certain longitudinal momentum fraction at resolution scales.

algorithms (see also **Signal Modelling** in Table 2.3).

To estimate systematic uncertainties on the modelling in an analysis, a set of MC samples with varied parameters is used to make new predictions for the process under study. Because each of these new simulations makes a different particle-level prediction, each generated event must pass a detector simulation which is computationally time consuming. Some uncertainties like the one on μ_R and μ_F can already be estimated using a re-weighting of the nominal MC simulation.

A new approach to estimate systematic uncertainties on the scale choice in the genertion of MC events has recently been developed [7]. The uncertainties are estimated by re-weighting the nominal MC simulation. For each generated event, a vector of alternative weights is provided for the uncertainty variations. The estimation of modelling uncertainties via reweighting is computationaly less expensive than generating new samples for each uncertainty. For the first time, the scale uncertainties are correlated between parton shower and PDF. The re-weighting also preserves the physical splittings in the parton shower and the total cross section.

4.2 Monte Carlo samples

The studies presented in this thesis focus on $t\bar{t}$ MC samples and the systematic uncertainties due to variations of the parton shower. The generator is Powheg+Pythia8: Powheg is used for the matrix element, Pythia8 for the showering and hadronisation.

The old approach to evaluate scale uncertainties was, to make just individual changes of Var3c for intial state radiation (ISR) and α_S for final state radiation (FSR).

The new approach is to use kernel splitting weights, i.e. each splitting in the shower is evaluated for changes in α_S^{FSR} (strong coupling constant). This is done for each kind of splitting individually. During the splitting four variations are used to separate different splitting situations. Table 4.1 shows the four variations and the meaning of them.

in particular, the meaning of X in X2XG is that the bottom quark or top quark since the number of flavours have been adjusted to be included in Q (u/d/s/c) to be 4 rather than 5. Therefore X2XG could be simply considered as a gluon bremsstrahlung off bottom quark or top quark.

variation	splitting situation	meaning of variation
G2GG	$g \to gg$	one gluon splits into two gluons
G2QQ	$g \to q\bar{q}$	one gluon splits into quark and antiquark pairs
Q2QG	$q \to qg$	one quark splits into same type quark and gluon
X2XG	$x \to xg$	other types of particles split into same type particle and gluon

Table 4.1: The name and the meaning of four variations used in new approach.

The old approach didn't consider the different weights of variations, which could cause larger uncertainties comparing to the new approach because the new approach considers correlations between the scale changes in ISR and FSR. Hence, it is necessary to deeply study the uncertainty contribution from different variations using new samples and compare with old samples.

5 Comparison between the FSR and ISR uncertainties estimation in old and new approach

The study focuses on the lepton+jets selection of $t\bar{t}$ events with one lepton (electron or muon) and 4 jets in the final state (on reconstruction level). The analysis focuses mainly on H_T plots and N_{jets} plots, in which H_T is defined as the scalar sum of all transverse momenta of jets, leptons and missing transverse momentum, N_{jets} gives the number of jets in each event. N_{jets} is especially sensitive to changes of additional radiation from ISR and FSR.

5.1 Comparison between up and down impact of each variation in ISR and FSR

In this section, the comparison of differences between up and down variations of both ISR and FSR have been processed. The purpose is to explore the differences between up and down variations in different lepton categories and for different kinematic variables and further potential influence on the total histograms.

5.1.1 Explanation

In this section, always the "up" component is considered as the base histogram, so in ratio plots the ratio is always "dn/up", which means "dn" histogram have been divided by "up" histogram to get the relative difference between them.

In this section, the total uncertainties in each histogram will be calculated to get the total uncertainties of each variation. The total histogram uncertainties are calculated by linearly summing the uncertainties between up and down of variation in each bin. This

is shown at the legend of each plot as " histo total uncertainty ".
During the calculation selections should also be made because for some bins only "up" or "down" exist, in this case the bin should be selected out of calculation otherwise the uncertainty of this bin is not the difference between "up" and "down", but the bin content of "up" or "down". Then the uncertainty would increase giantly.

In this section, the ratio total uncertainties will also be calculated to get the relative uncertainties of the ratio plots. The ratio total uncertainties are calculated by adding the uncertainties between up and down of each bin in quadrature and are then divided by the total number of bins. This is shown at the legend of each plot as "ratio total uncertainty".

Because for different variation the ratio of "dn/up" is different, so for a certain ratio range some plots could be out of range, while the others do not show much variation in this certain range. Therefore, 3 ratio ranges are selected for both large and small uncertainties, i.e. [0.9:1.1] , [0.95:1.05], [0.99:1.01]. These three ratio ranges are used in order to take into consideration the spread of the ratio down/up values of different variations, and to make the plots more meaningful.

5.1.2 H_T and N_{jets} multiplicity distributions for individual variations of both ISR and FSR for single electron

Electron-G2GG

Here the N_{jets} and H_T comparison of G2GG variations between up and down in the single electron channel for ISR and FSR is shown:

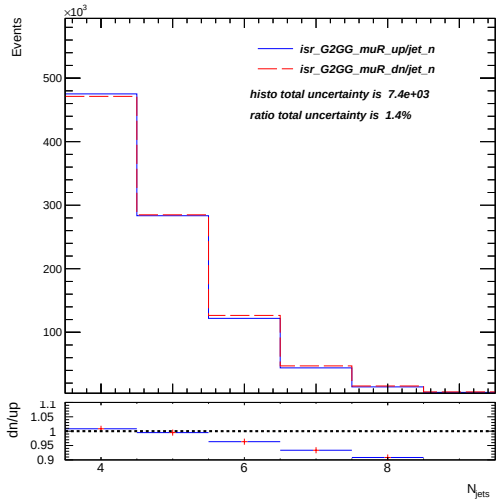

Figure 5.1: N_{jets} multiplicity distributions for the ISR/G2GG variation in e+jet events.

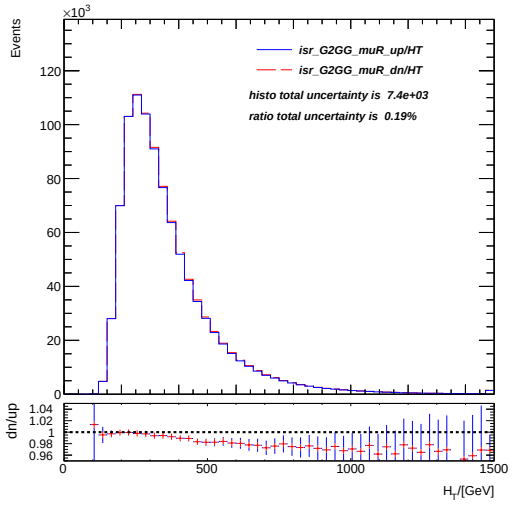

Figure 5.2: H_T distributions for the ISR/G2GG variation in e+jet events.

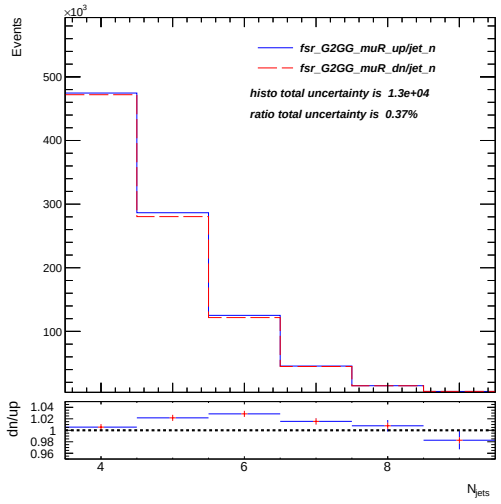

Figure 5.3: N_{jets} multiplicity distributions for the FSR/G2GG variation in e+jet events.

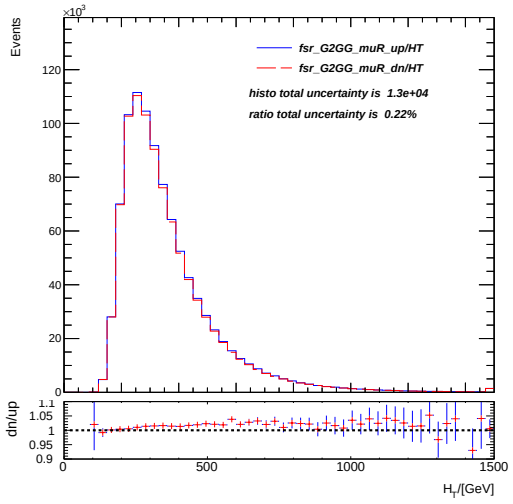

Figure 5.4: H_T distributions for the FSR/G2GG variation in e+jet events.

For the ISR variation, the difference of "up' and "down" in the N_{jets} plot has increased with increasing N_{jet} and the uncertainty increases from 5% at N=6 to over 10% at N above 8, and in the H_T plot the difference increases with increasing transverse momentum.

For the FSR variation, the difference of "up" and "down" in the N_{jets} plot has its largest difference at N=6 around 3%, and in the H_T plot the difference increase to over 5% at around 1300 GeV.

Electron-G2QQ

Here the N_{jets} and H_T comparison of G2QQ variations between up and down in the single electron channel for ISR and FSR is shown:

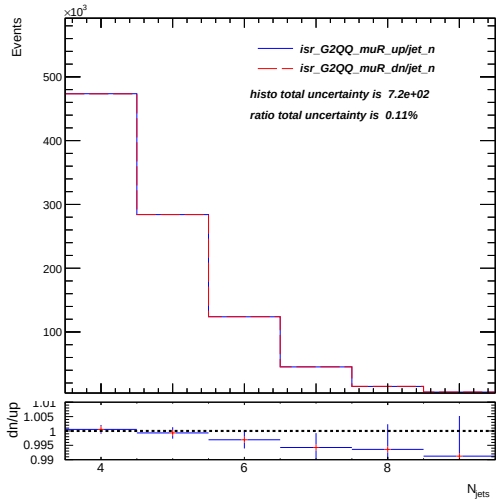

Figure 5.5: N_{jets} multiplicity distributions for the ISR/G2QQ variation in e+jet events.

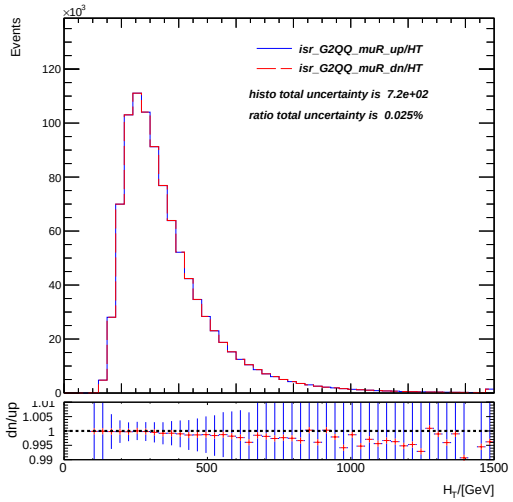

Figure 5.6: H_T distributions for the ISR/G2QQ variation in e+jet events.

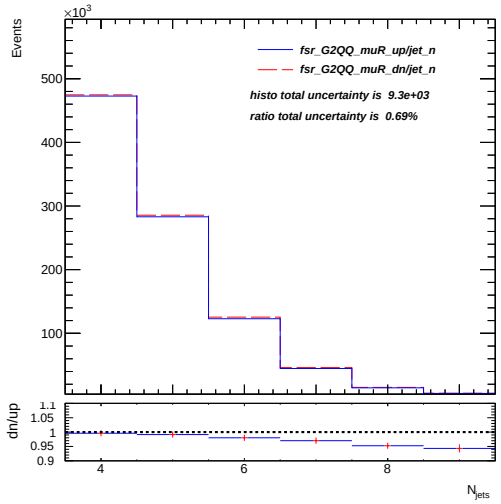

Figure 5.7: N_{jets} multiplicity distributions for the FSR/G2QQ variation in e+jet events.

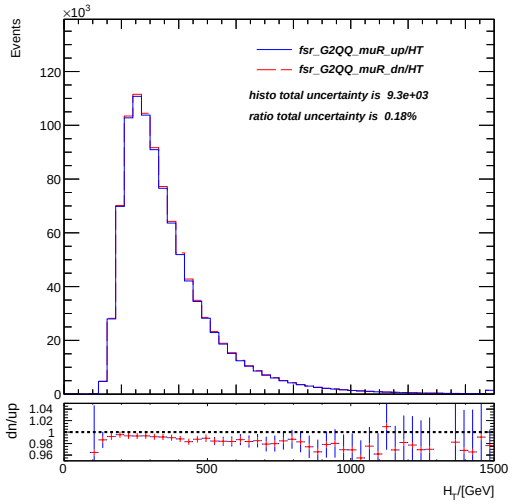

Figure 5.8: H_T distributions for the FSR/G2QQ variation in e+jet events.

For the ISR variation, the difference of "up' and "down" in the N_{jets} plot has increased as N increases and reaches 1% at N=9. And in the H_T plot the differences are relatively small, most below 0.5%.

For the FSR variation, the difference of "up" and "down" in the N_{jets} plot has increased with increasing N and reach around 6% at N=9, and in the H_T plot the difference increases

from 1% at beginning to 4% at over 1000 GeV.

Electron-Q2QG

Here the N_{jets} and H_T comparison of Q2QG variations between up and down in the single electron channel for ISR and FSR is shown:

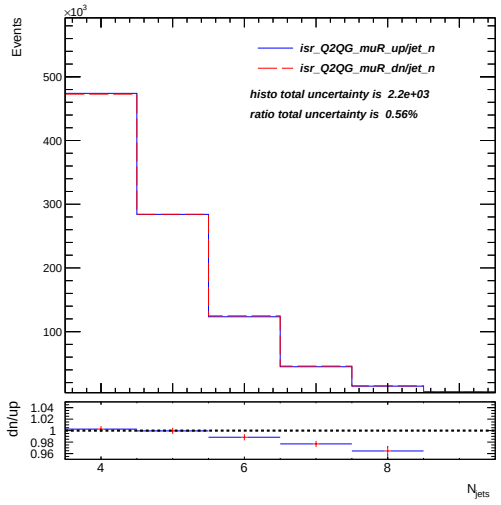

Figure 5.9: N_{jets} multiplicity distributions for the ISR/Q2QG variation in e+jet events.

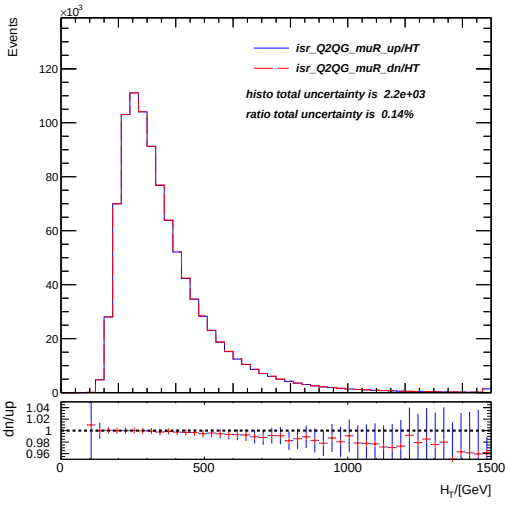

Figure 5.10: H_T distributions for the ISR/Q2QG variation in e+jet events.

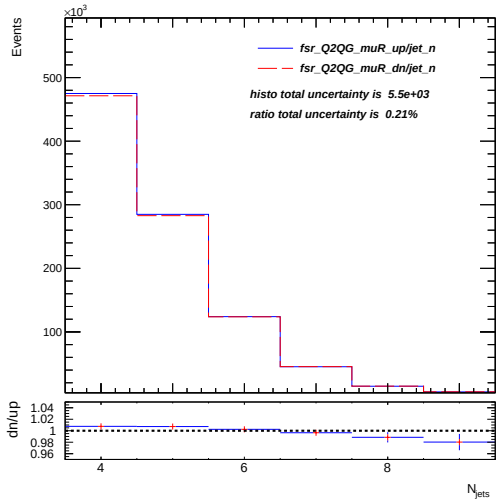

Figure 5.11: N_{jets} multiplicity distributions for the FSR/Q2QG variation in e+jet events.

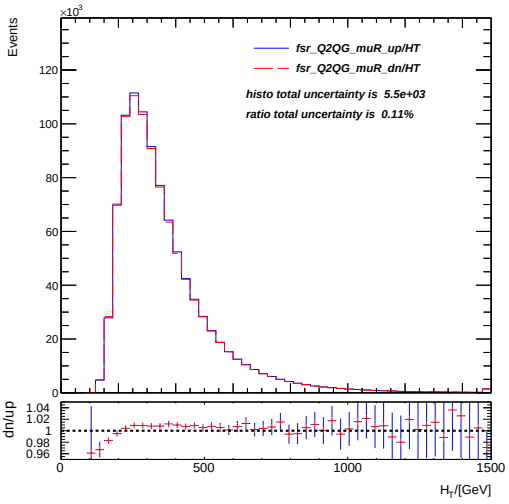

Figure 5.12: H_T distributions for the FSR/Q2QG variation in e+jet events.

For the ISR variation, the difference of "up' and "down" in the N_{jets} plot has increased with increasing N and over 5% at N=9. And in the H_T plot the difference increases with transverse momentum increase from below 1% at beginning to 4% at around 1500 GeV.

For the FSR variation, the difference of "up" and "down" in the N_{jets} plot has increased with nincreasing N and reaches around 2% at N=9, and in the H_T plot the difference decreases at beginning (below 200 GeV) from 4% to less 1 % and then increase to around 4 % above 1000 GeV.

Electron-X2XG

Here the N_{jets} and H_T comparison of X2XG variations between up and down in the single electron channel for ISR and FSR is shown:

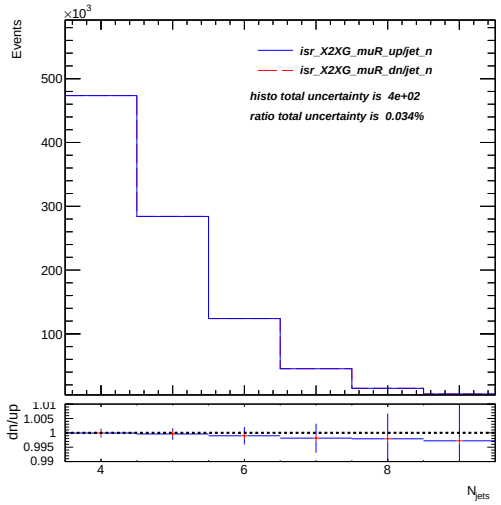

Figure 5.13: N_{jets} multiplicity distributions for the ISR/X2XG variation in e+jet events.

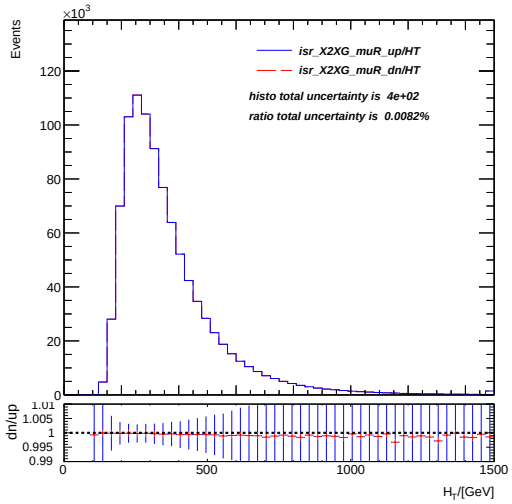

Figure 5.14: H_T distributions for the ISR/X2XG variation in e+jet events.

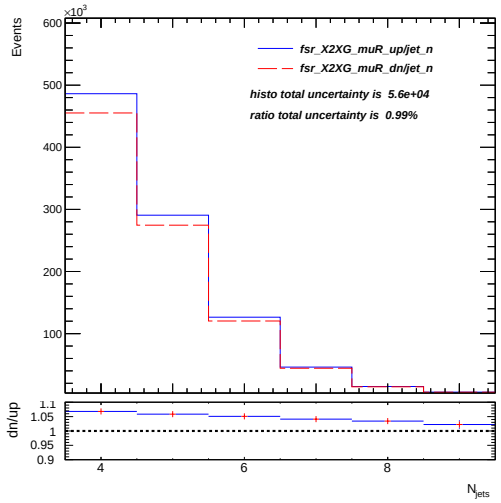

Figure 5.15: N_{jets} multiplicity distributions for the FSR/X2XG variation in e+jet events.

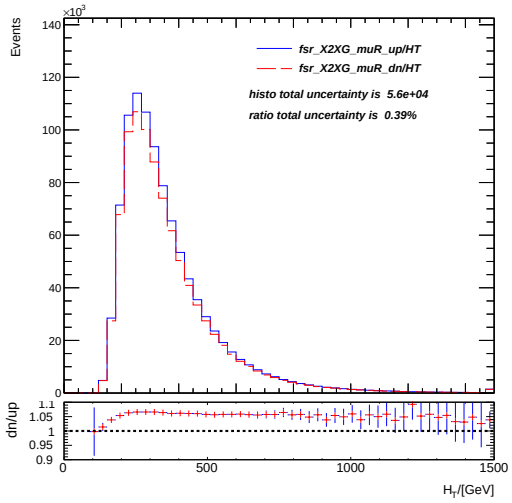

Figure 5.16: H_T distributions for the FSR/X2XG variation in e+jet events.

For the ISR variation, the difference of "up' and "down" in both the N_{jets} and the H_T plot are extremely small that they do not show any uncertainties. Both of the uncertainties are below 0.2%.
In FSR, the difference of "up" and "down" in the N_{jets} plot has decreased with increasing N from 8% at N=4 to 2% at N=9, and in the H_T plot the difference rapidly increases to 7% around 200 GeV and are stable above 5% until 1500 GeV.

5.1.3 H_T and N_{jets} multiplicity distributions for individual variations of both ISR and FSR for single muon

Muon-G2GG

Here the N_{jets} and H_T comparison of G2GG variations between up and down in the single muon channel for ISR and FSR is shown:

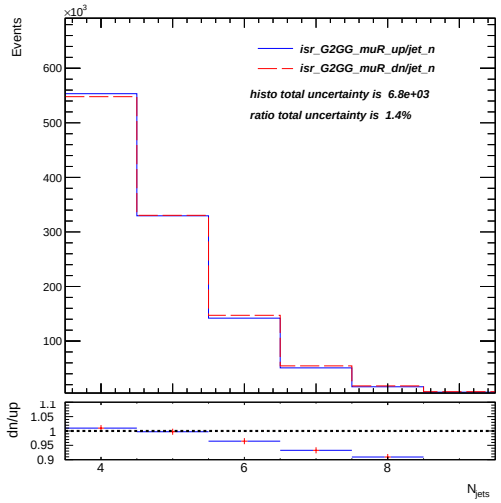

Figure 5.17: N_{jets} multiplicity distributions for the ISR/G2GG variation in μ+jet events.

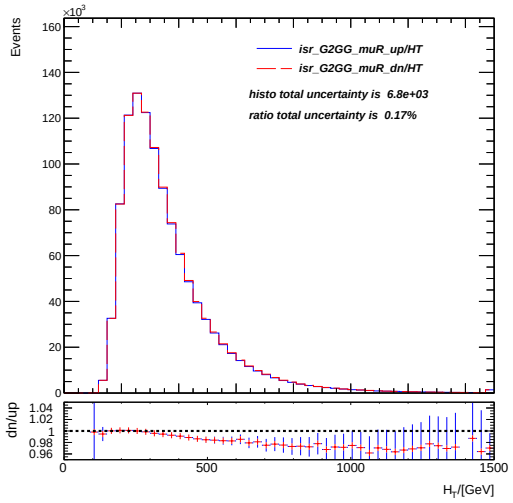

Figure 5.18: H_T distributions for the ISR/G2GG variation in μ+jet events.

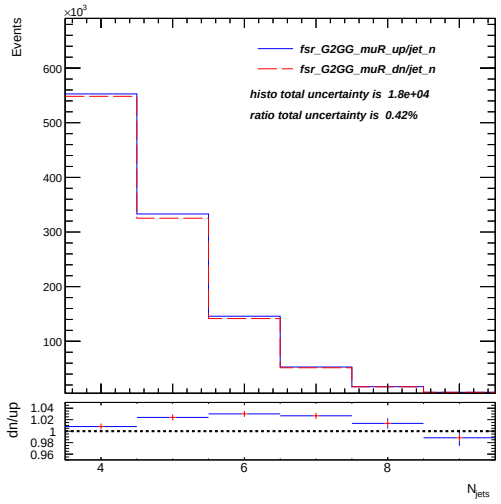

Figure 5.19: N_{jets} multiplicity distributions for the FSR/G2GG variation in μ+jet events.

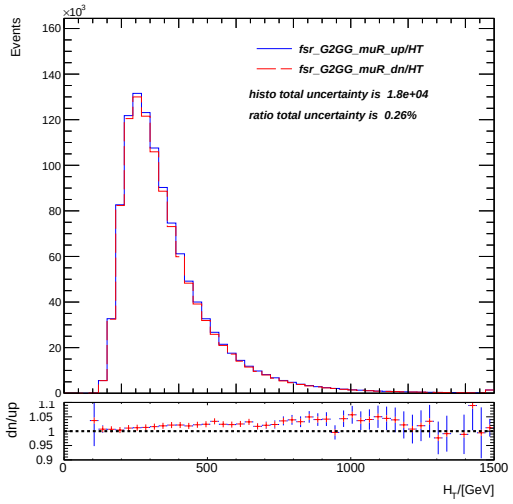

Figure 5.20: H_T distributions for the ISR/G2GG variation in μ+jet events.

For the ISR variation, the difference of "up' and "down" in the N_{jets} plot has increased with increasing N and the uncertainty increases from 5% at N=6 to over 10% at above 8, and in the H_T plot the difference increases with transverse momentum increase to around 4% until 1500 GeV.

For the FSR variation, the difference of "up" and "down" in the N_{jets} plot has its largest difference at N=6 around 3%, and in H_T plot the difference increases with increasing transverse momentum and over 4% around 1000 GeV.

Muon-G2QQ

Here the N_{jets} and H_T comparison of G2QQ variations between up and down in the single muon channel for ISR and FSR is shown:

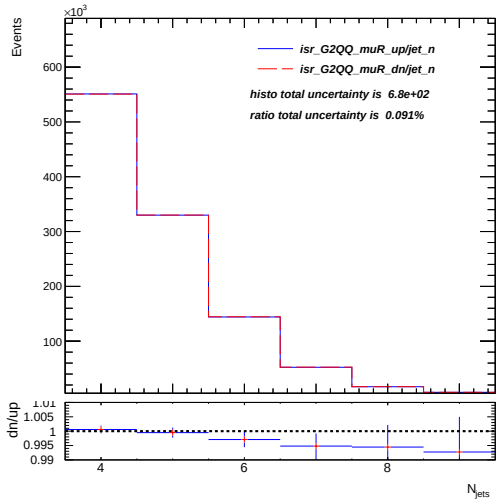

Figure 5.21: N_{jets} multiplicity distributions for the ISR/G2QQ variation in μ+jet events.

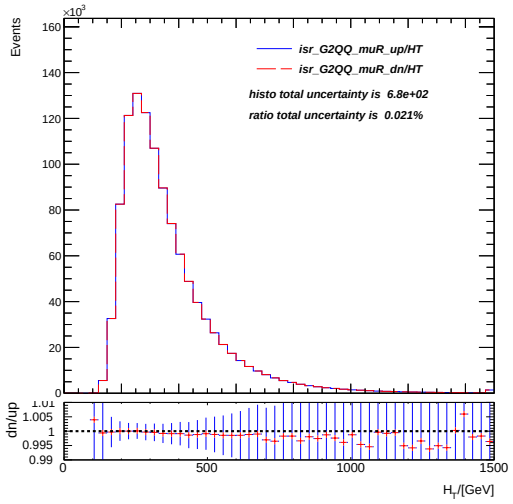

Figure 5.22: H_T distributions for the ISR/G2QQ variation in μ+jet events.

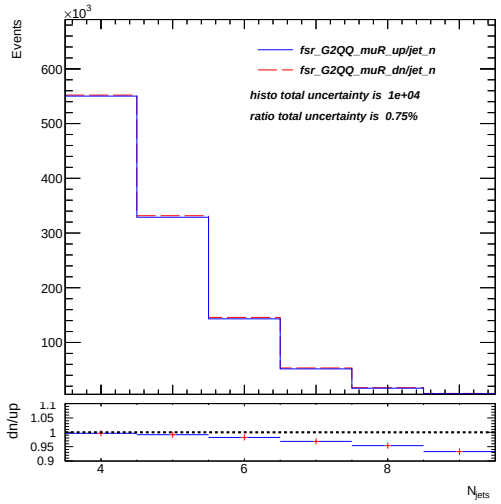

Figure 5.23: N_{jets} multiplicity distributions for the FSR/G2QQ variation in μ+jet events.

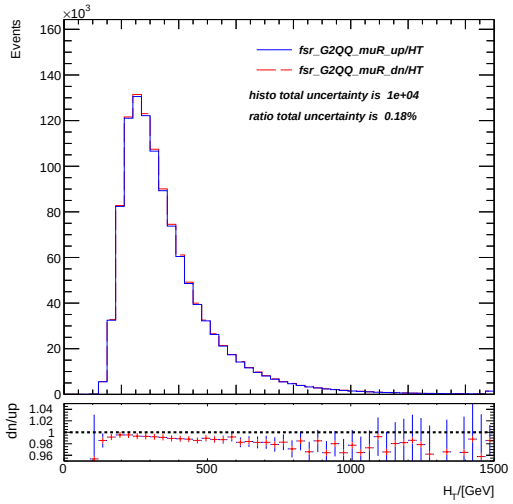

Figure 5.24: H_T distributions for the FSR/G2QQ variation in μ+jet events.

For the ISR variation, the difference of "up' and "down" in the N_{jets} plot has increased as N increases and around 0.8% at N=9. And in the H_T plot the differences are relatively small, i.e. below 0.5%.

For the FSR variation, the difference of "up" and "down" in the N_{jets} plot has increased with increasing N and over 5% at N=9, and in the H_T plot the differences increase from 1% at beginning to 5% at over 1000 GeV.

Muon-Q2QG

Here the N_{jets} and H_T comparison of Q2QG variations between up and down in the single muon channel for ISR and FSR is shown:

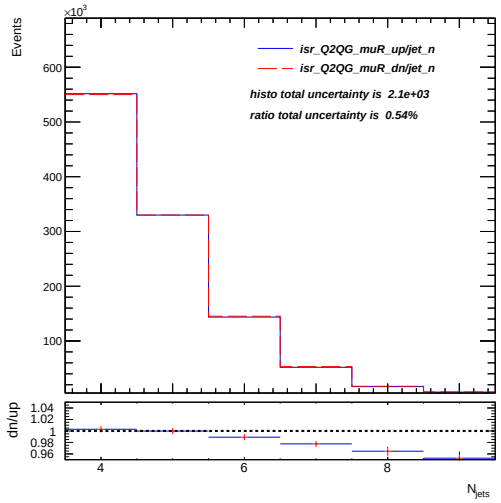

Figure 5.25: N_{jets} multiplicity distributions for the ISR/Q2QG variation in μ+jet events.

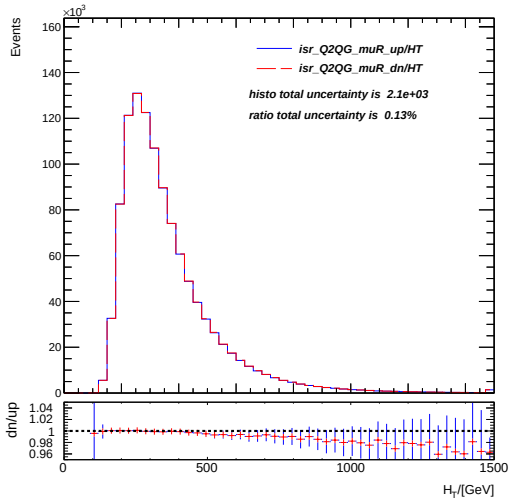

Figure 5.26: H_T distributions for the ISR/Q2QG variation in μ+jet events.

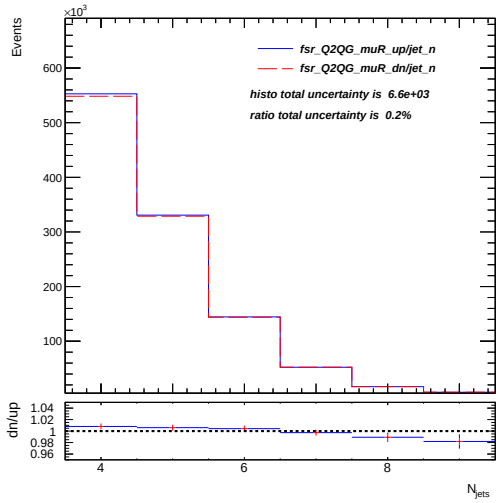

Figure 5.27: N_{jets} multiplicity distributions for the FSR/Q2QG variation in μ+jet events.

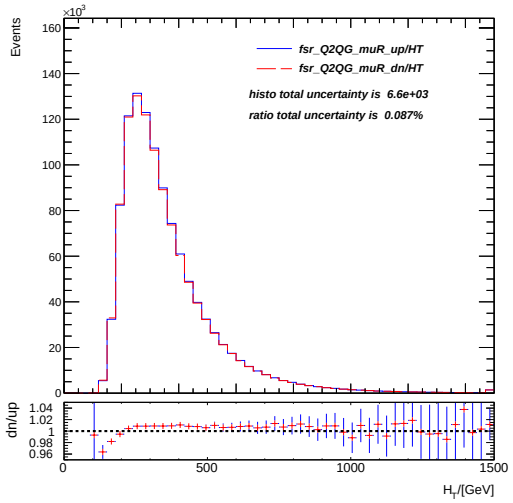

Figure 5.28: H_T distributions for the FSR/Q2QG variation in μ+jet events.

For the ISR variation, the difference of "up' and "down" in the N_{jets} plot has increased as n increases and around 5% at N=9. And in the H_T plot the difference increases with increasing transverse momentum from below 1% at low H_T to 4% at around 1500 GeV. For the FSR variation, the differences of "up" and "down" in the N_{jets} plot are relatively small and reach around 2% at N=9, and in the H_T plot the difference decreases at

$H_T < 200$ GeV from 4% to less 1 % and then increases to around 2 % at above 1000 GeV.

Muon-X2XG

Here the N_{jets} and H_T comparison of X2XG variations between up and down in the single muon channel for ISR and FSR is shown:

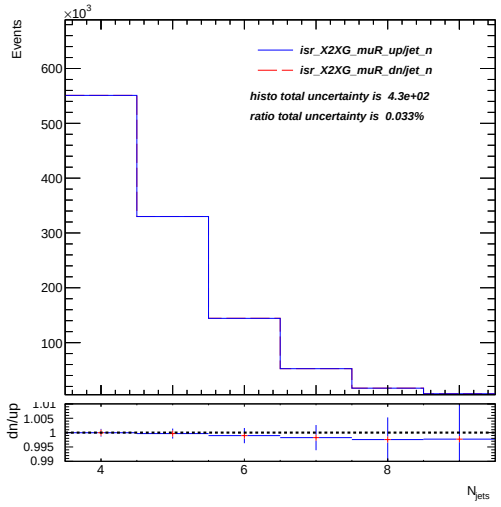

Figure 5.29: N_{jets} multiplicity distributions for the ISR/X2XG variation in μ+jet events.

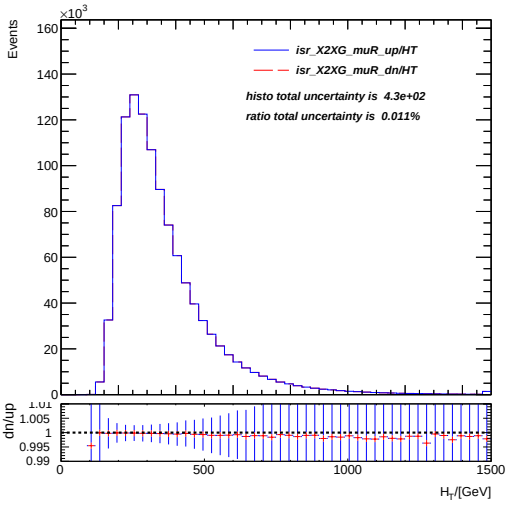

Figure 5.30: H_T distributions for the ISR/X2XG variation in μ+jet events.

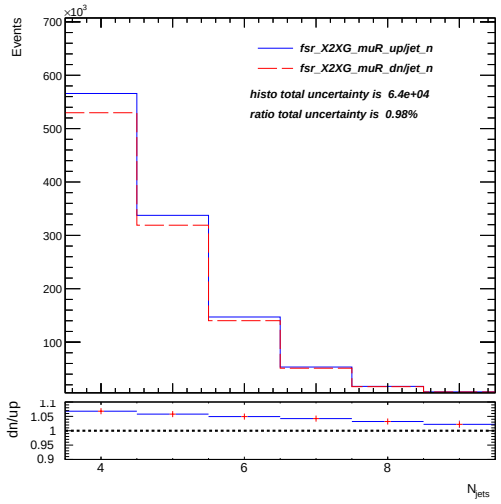

Figure 5.31: N_{jets} multiplicity distributions for the FSR/X2XG variation in μ+jet events.

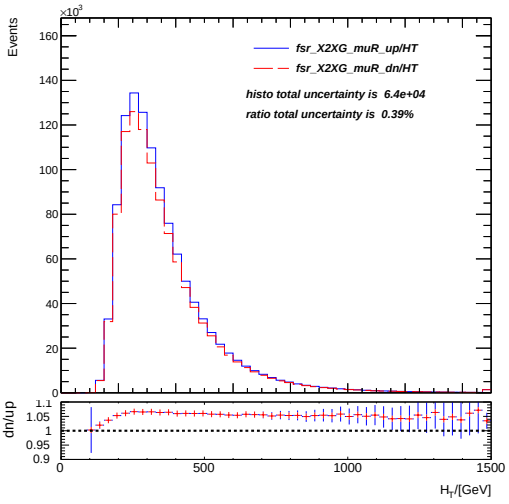

Figure 5.32: H_T distributions for the FSR/X2XG variation in μ+jet events.

For the ISR variation, the difference of "up' and "down" in both the N_{jets} and the H_T plot are extremely small that they do not show any uncertainties. Both of the uncertainties are below 0.2%.

For the FSR variation, the difference of "up" and "down" in the N_{jets} plot has decreased with increasing N from 8% at N=4 to 2% at N=9, and in the H_T plot the difference rapidly increases at beginning to 7% at around 1200 GeV and are stable above 5% at until 1500 GeV.

5.1.4 Discussion

The maximal uncertainties between up and down in both N_{jets} and H_T plots of 4 variations of ISR and FSR in e+jet event and μ+jet event are summarised in Table 5.1.

variation	e+jet N_{jets} plot	μ+jet N_{jets} plot	e+jet H_T plot	μ+jet H_T plot
ISR-G2GG	over 10%	over 10%	around 4%	around 4%
FSR-G2GG	under 3%	around 3%	over 5%	over 4%
ISR-G2QQ	under 1%	around 0.8%	under 0.5%	under 0.5%
FSR-G2QQ	around 6%	over 5%	around 4%	around 5%
ISR-Q2QG	over 5%	around 5%	around 4%	around 4%
FSR-Q2QG	around 2%	around 2%	around 4%	around 2%
ISR-X2XG	around 0.2%	around 0.2%	under 0.2%	under 0.2%
FSR-X2XG	around 8%	around 8%	above 5%	above 5%

Table 5.1: Summarising table of maximal uncertainties between up and down of each variation of ISR and FSR in e+jet or μ+jet events.

Comparing the uncertainties in e+jet and μ+jet events at same variation and also the shape of them in plots, it can be concluded that in general single electron and single muon events have similar shape for both N_{jets} and H_T plots for ISR and FSR variation. The uncertainties of them do not differ too much. So electron and muon could be included as single lepton in the analysis.

This section shows how the difference between "up" and "down" single lepton is related to different jet multiplicity and to the transverse momentum of jets. To get which variation has contributed the most uncertainties to the total part, it is required to compare between 4 variations.

5.2 Comparison of histogram total uncertainty and ratio total uncertainty between 4 variations

In this section, the comparison between 4 variations about the difference of "up" and "down" in the single lepton channel will be presented. The aim is to find the variation which has the largest uncertainty among them.

Only by comparing the shape and observing the the ratio plots with eyes sometimes it is difficult to decide which has larger and which has smaller uncertainties. Different ratio range cause also difficulties to compare with eyes. Therefore mathematical support is needed to make the results more convincing.

5.2.1 Comparing and Discussion

The histogram total uncertainty and the ratio total uncertainty of 4 variations of ISR and FSR are summarised in Table 5.2. The calculated histogram total uncertainty and ratio total uncertainty values are shown in the plots in section 5.1.

For both N_{jets} and H_T plots of electron and muon for the ISR variation, G2GG contribute the most uncertainty to the total in ISR, while Q2QG has the second largest impact and G2QQ and X2XG the third and the fourth largest impact to the total. X2XG has really small uncertainties compared to other variations that it almost does not show any variations.
For both N_{jets} and H_T plots of electron and muon for the FSR variation: X2XG contribute the most largest impact to total and Q2QG the smallest impact. For N_{jets} plots G2QQ has the second largest impact to total and for H_T plots G2GG has the second largest impact, G2GG has the third largest impact for N_{jets} plots and G2QQ for H_T plots.

5.3 Comparison of nominal histograms with modified error in the new approach

In this section, the comparison between 4 variations to the nominal histograms will be processed to see the different impact of 4 variations and how much uncertainties they have contributed to the total uncertainties.

5.3.1 Explanation

In this section, "nominal" histograms are used as the histograms without any variations. As analysed before, "ISR-X2XG" does not show variations for both single electron and muon, so it could be considered as nominal during the analysis. This has been done because the nominal histograms were not available for technical reasons.

What have to pay attention in this section is the error bars in the histograms and ratio plots:
In histograms, the error bar means the difference between variations and nominal. For each variation, the difference are the sum of distance between "up" and "nominal" and the distance between "down" and "nominal". If both "up" and "down" are larger or smaller than "nominal", then only the one with largest distance would be considered as the difference, the other one would be ignored. The "total histo uncertainty" is the sum of all differences on each bin.
In ratio plots, error bars stands for the relative uncertainties, i.e. divide the difference between variations and nominal by the bin content.

Sometimes the error bars and the axis scale could overlap especially in N_{jets} plot, which has to be considered if observing the plots by eye.

5.3.2 Comparison of variations contributions to the uncertainty on nominal histograms in lepton+jets event

Electron-ISR-N_{jets}

Here the comparison of N_{jets} plots of 4 ISR variations in the single electron channel is shown.

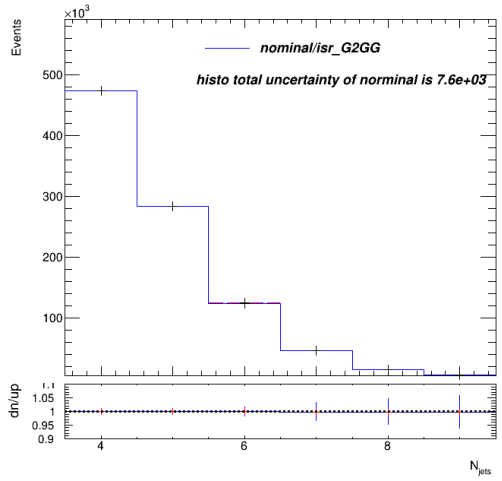

Figure 5.33: N_{jets} multiplicity distributions with modified error on nominal histograms for the ISR/G2GG variation in the e+jet events.

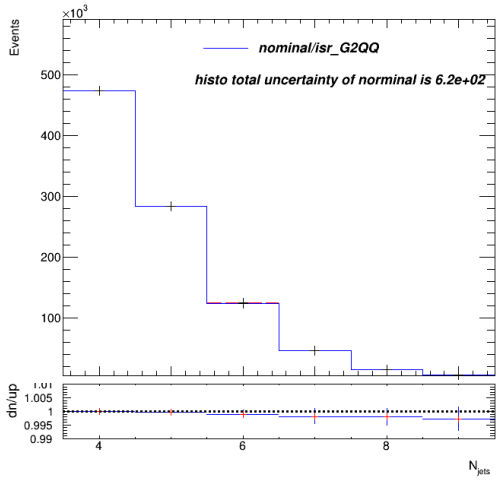

Figure 5.34: N_{jets} multiplicity distributions with modified error on nominal histograms for the ISR/G2QQ variation in the e+jet events.

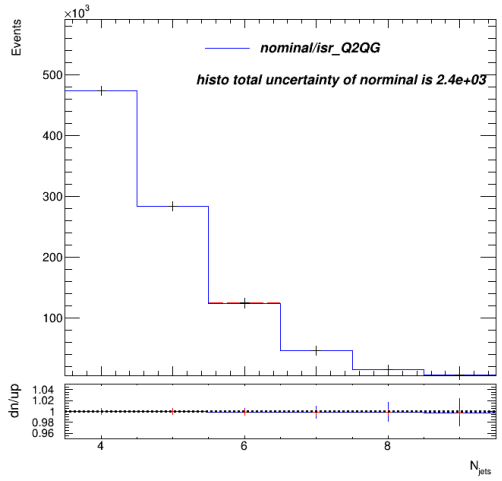

Figure 5.35: N_{jets} multiplicity distributions with modified error on nominal histograms for the ISR/Q2QG variation in the e+jet events.

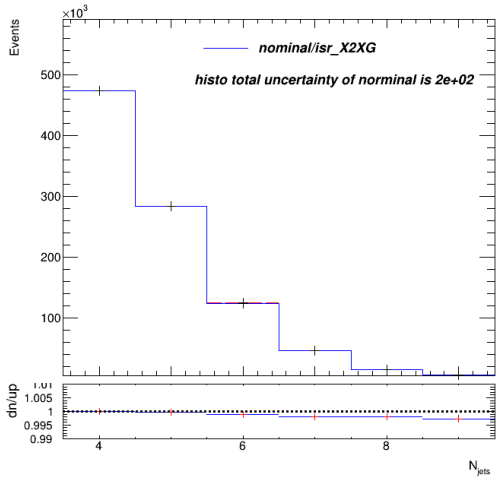

Figure 5.36: N_{jets} multiplicity distributions with modified error on nominal histograms for the ISR/X2XG variation in the e+jet events.

Comparing the histogram total uncertainties and error bars in ratio plots, the relation of 4 variations contribution to the uncertainty on nominal histograms could be shown below:

For electron-ISR-N_{jets}: $G2GG > Q2QG > G2QQ > X2XG$

Electron-ISR-H_T

Here the comparison of H_T plots of 4 variations impact into total of single electron in ISR are shown:

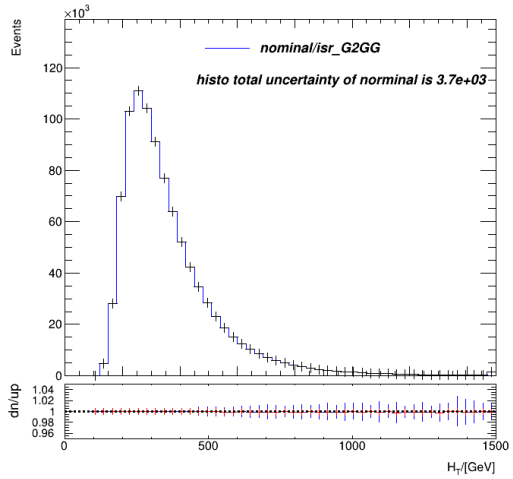

Figure 5.37: H_T distributions with modified error on nominal histograms for the ISR/G2GG variation in the e+jet events.

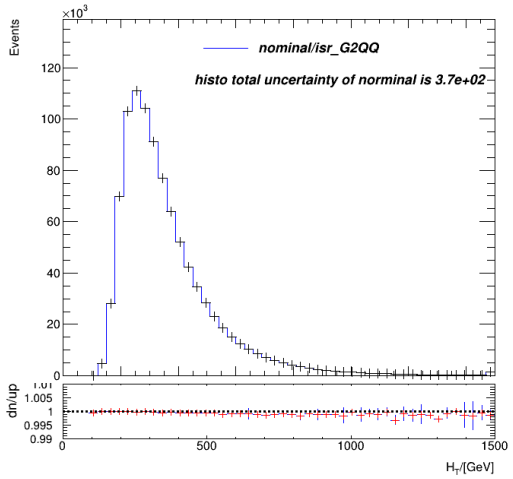

Figure 5.38: H_T distributions with modified error on nominal histograms for the ISR/G2QQ variation in the e+jet events.

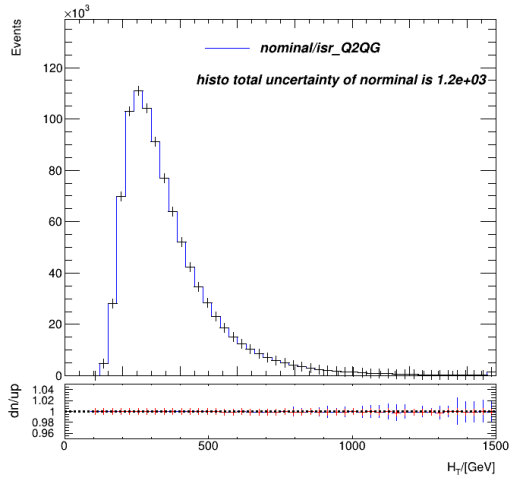

Figure 5.39: H_T distributions with modified error on nominal histograms for the ISR/Q2QG variation in the e+jet events.

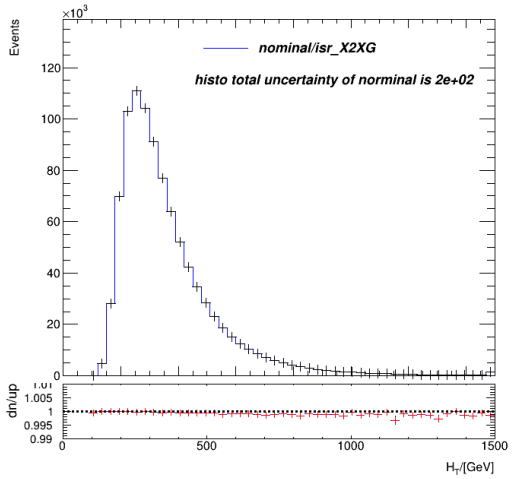

Figure 5.40: H_T distributions with modified error on nominal histograms for the ISR/X2XG variation in the e+jet events.

Comparing the histogram total uncertainties and error bars in ratio plots, the relation of 4 variations contribution to the uncertainty on nominal histograms could be shown below:

For electron-ISR-H_T: $G2GG > Q2QG > G2QQ > X2XG$

Electron-FSR-N_{jets}

Here the comparison of N_{jets} plots of 4 variations impact into total of single electron in FSR are shown:

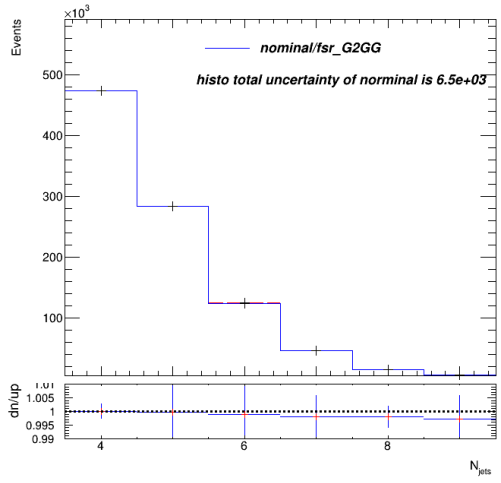

Figure 5.41: N_{jets} multiplicity distributions with modified error on nominal histograms for the FSR/G2GG variation in the e+jet events.

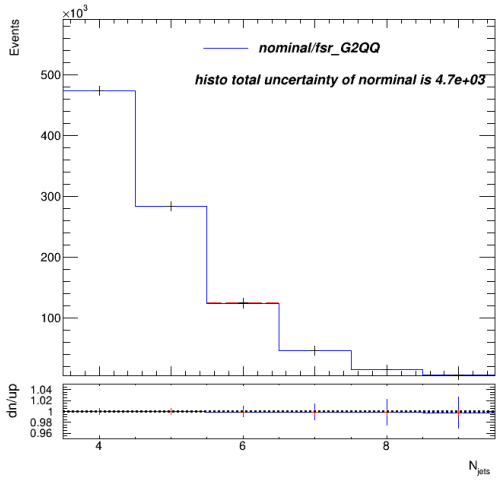

Figure 5.42: N_{jets} multiplicity distributions with modified error on nominal histograms for the FSR/G2QQ variation in the e+jet events.

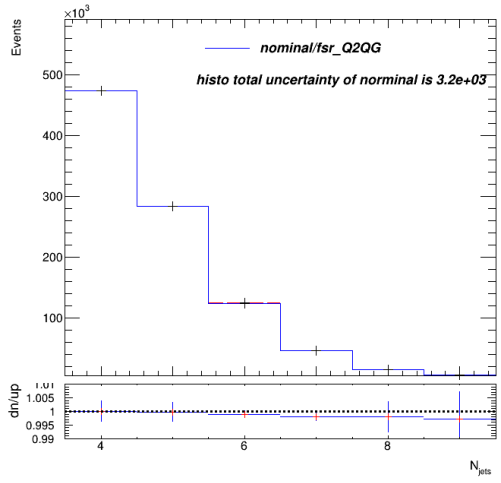

Figure 5.43: N_{jets} multiplicity distributions with modified error on nominal histograms for the FSR/Q2QG variation in the e+jet events.

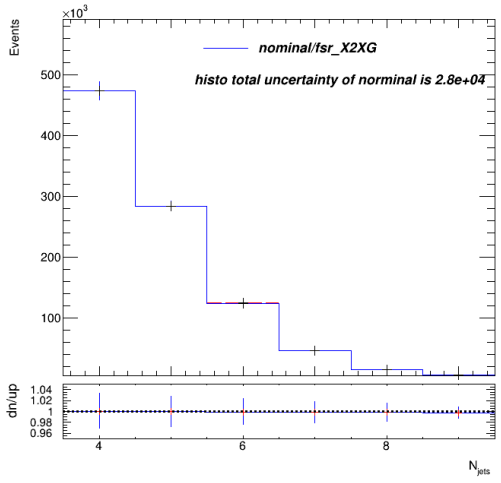

Figure 5.44: N_{jets} multiplicity distributions with modified error on nominal histograms for the FSR/X2XG variation in the e+jet events.

Comparing the histogram total uncertainties and error bars in ratio plots, the relation of 4 variations contribution to the uncertainty on nominal histograms could be shown below:

For electron-FSR-N_{jets}: $X2XG > G2GG > G2QQ > Q2QG$

Electron-FSR-H_T

Here the comparison of H_T plots of 4 variations impact into total of single electron in FSR are shown:

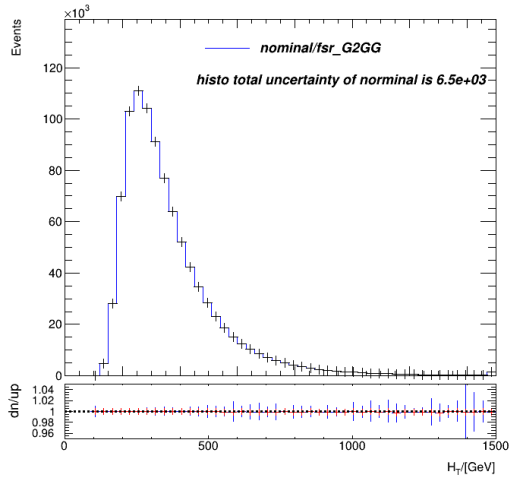

Figure 5.45: H_T distributions with modified error on nominal histograms for the FSR/G2GG variation in the e+jet events.

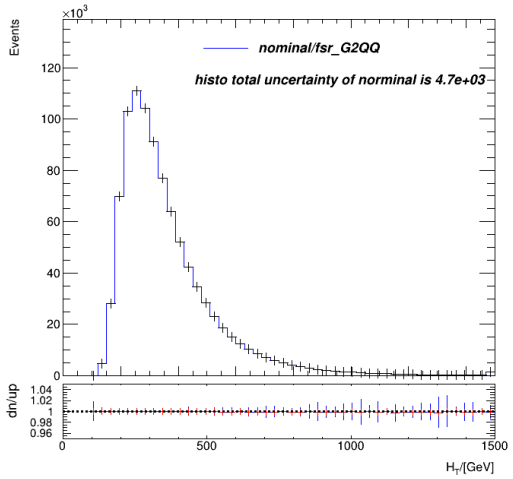

Figure 5.46: H_T distributions with modified error on nominal histograms for the FSR/G2QQ variation in the e+jet events.

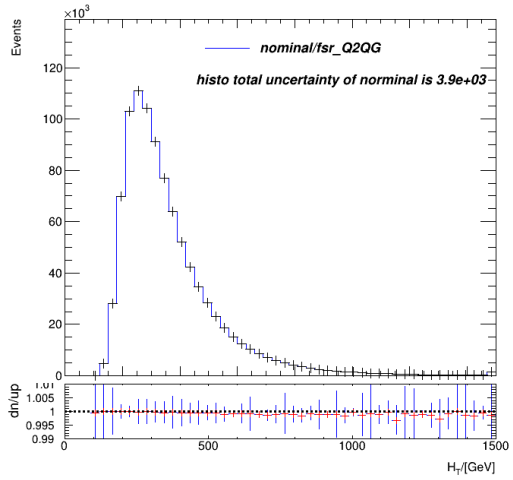

Figure 5.47: H_T distributions with modified error on nominal histograms for the FSR/Q2QG variation in the e+jet events.

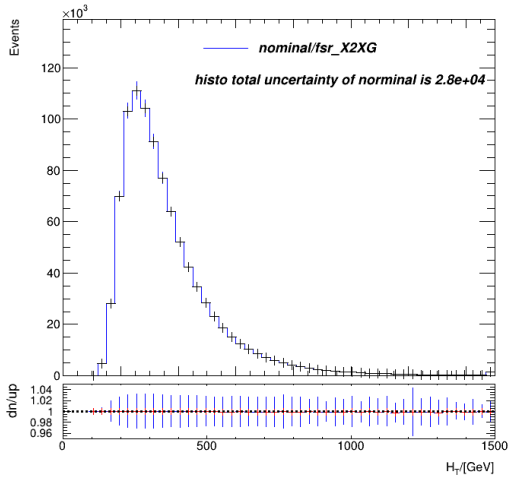

Figure 5.48: H_T distributions with modified error on nominal histograms for the FSR/X2XG variation in the e+jet events.

Comparing the histogram total uncertainties and error bars in ratio plots, the relation of 4 variations contribution to the uncertainty on nominal histograms could be shown below:

For electron-FSR-H_T: $X2XG > G2GG > G2QQ > Q2QG$

Muon-ISR-N_{jets}

Here the comparison of N_{jets} plots of 4 variations impact into total of single muon in ISR are shown:

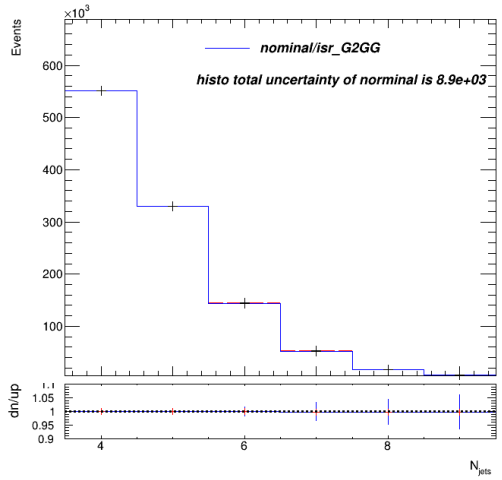

Figure 5.49: N_{jets} multiplicity distributions with modified error on nominal histograms for the ISR/G2GG variation in the μ+jet events.

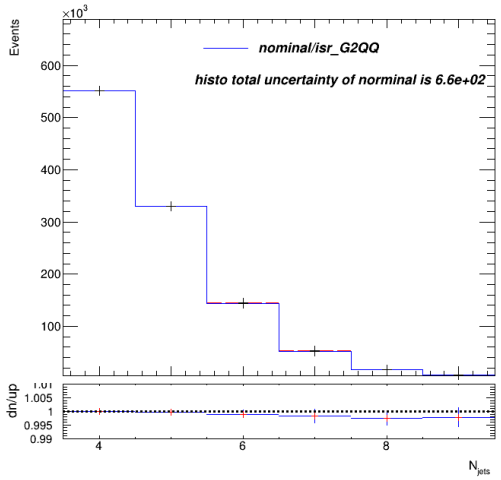

Figure 5.50: N_{jets} multiplicity distributions with modified error on nominal histograms for the ISR/G2QQ variation in the μ+jet events.

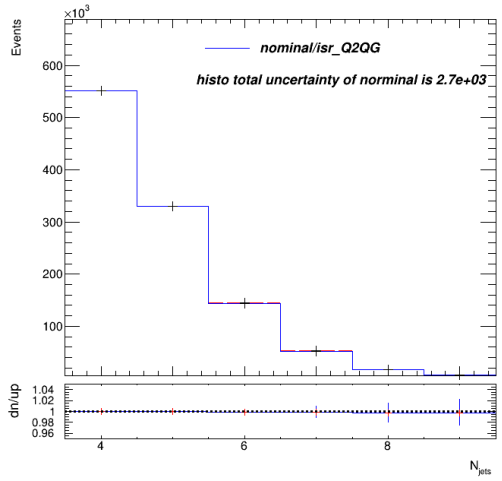

Figure 5.51: N_{jets} multiplicity distributions with modified error on nominal histograms for the ISR/Q2QG variation in the μ+jet events.

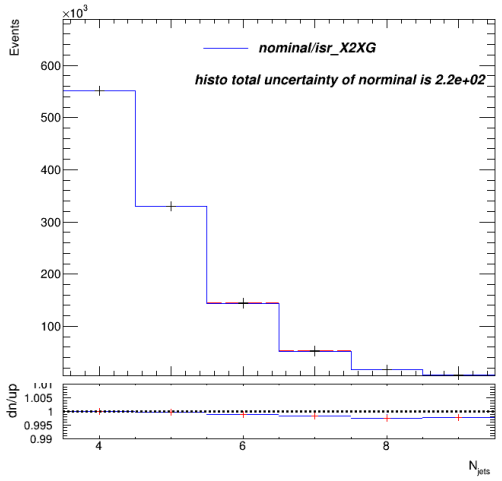

Figure 5.52: N_{jets} multiplicity distributions with modified error on nominal histograms for the ISR/X2XG variation in the μ+jet events.

Comparing the histogram total uncertainties and error bars in ratio plots, the relation of 4 variations contribution to the uncertainty on nominal histograms could be shown below:

For muon-ISR-N_{jets}: $G2GG > Q2QG > G2QQ > X2XG$

Muon-ISR-H_T

Here the comparison of H_T plots of 4 variations impact into total of single muon in ISR are shown:

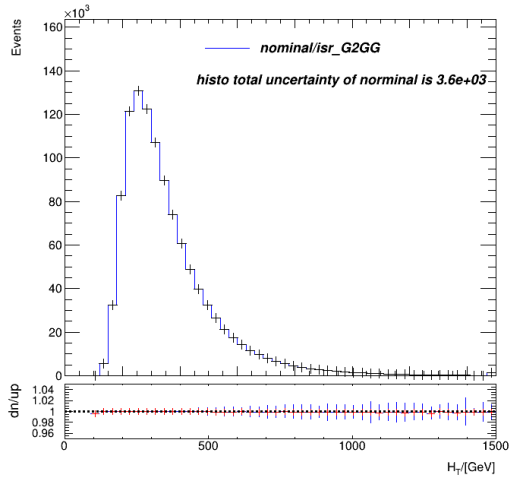

Figure 5.53: H_T distributions with modified error on nominal histograms for the ISR/G2GG variation in the μ+jet events.

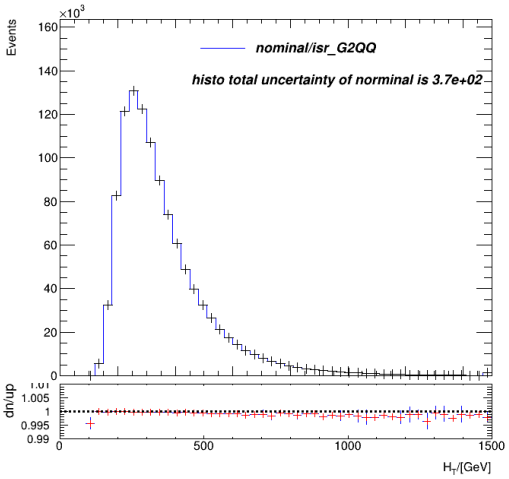

Figure 5.54: H_T distributions with modified error on nominal histograms for the ISR/G2QQ variation in the μ+jet events.

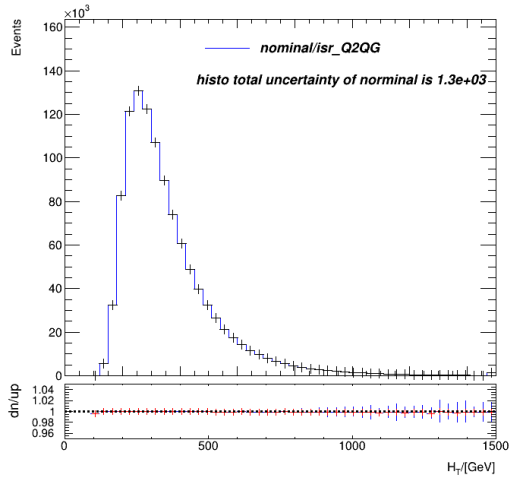

Figure 5.55: H_T distributions with modified error on nominal histograms for the ISR/Q2QG variation in the μ+jet events.

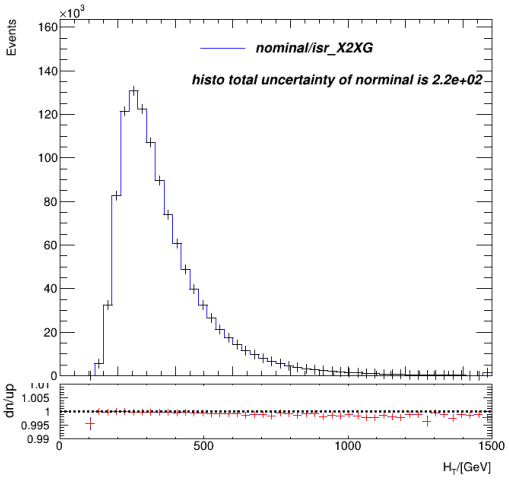

Figure 5.56: H_T distributions with modified error on nominal histograms for the ISR/X2XG variation in the μ+jet events.

Comparing the histo total uncertianties and error bars in ratio plots the relation of 4 variatons impact into total could be shown below:

For muon-ISR-H_T: $G2GG > Q2QG > G2QQ > X2XG$

Muon-FSR-N_{jets}

Here the comparison of N_{jets} 4 plots of 4 variations impact into total of single muon in FSR are shown:

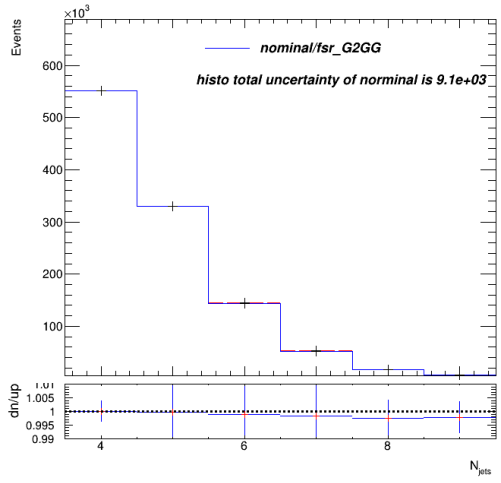

Figure 5.57: N_{jets} multiplicity distributions with modified error on nominal histograms for the FSR/G2GG variation in the μ+jet events.

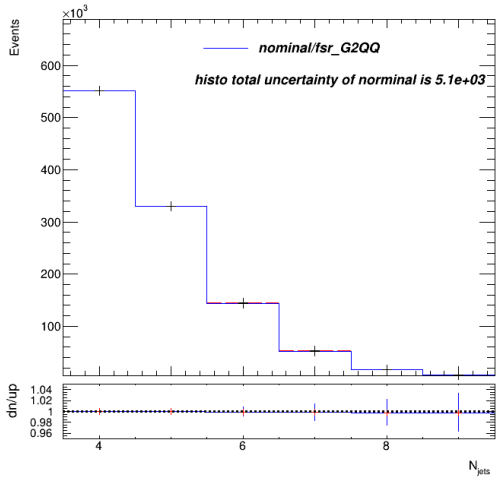

Figure 5.58: N_{jets} multiplicity distributions with modified error on nominal histograms for the FSR/G2QQ variation in the μ+jet events.

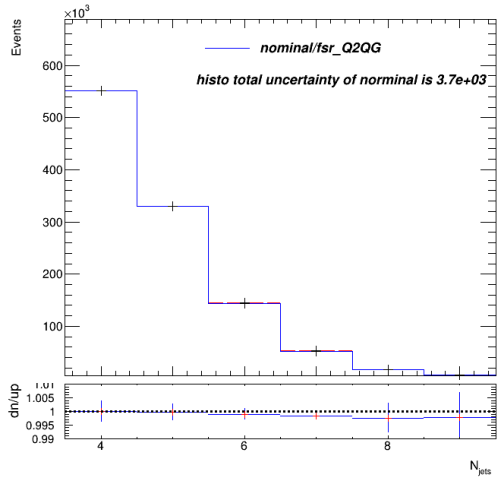

Figure 5.59: N_{jets} multiplicity distributions with modified error on nominal histograms for the FSR/Q2QG variation in the μ+jet events.

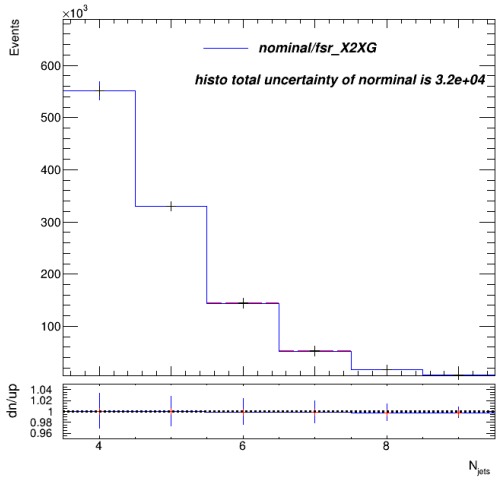

Figure 5.60: N_{jets} multiplicity distributions with modified error on nominal histograms for the FSR/X2XG variation in the μ+jet events.

Comparing the histogram total uncertainties and error bars in ratio plots, the relation of 4 variations contribution to the uncertainty on nominal histograms could be shown below:

For muon-FSR-N_{jets}: $X2XG > G2GG > G2QQ > Q2QG$

Muon-FSR-H_T

Here the comparison of H_T plots of 4 variations impact into total of single muon in FSR are shown:

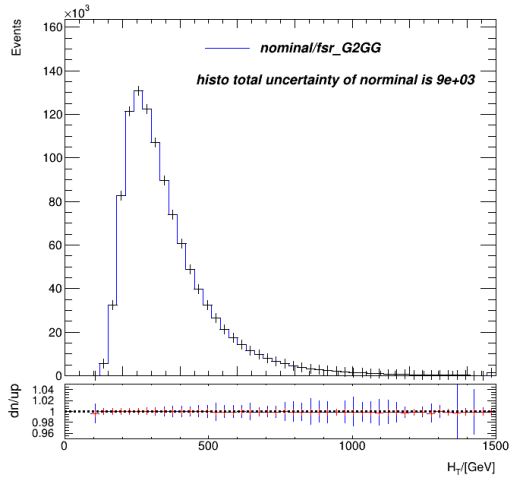

Figure 5.61: H_T distributions with modified error on nominal histograms for the FSR/G2GG variation in the μ+jet events.

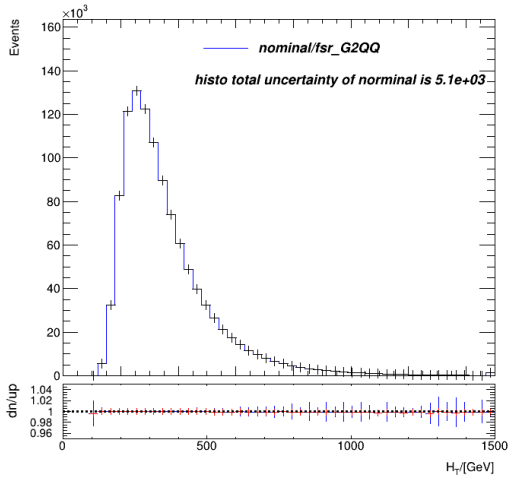

Figure 5.62: H_T distributions with modified error on nominal histograms for the FSR/G2QQ variation in the μ+jet events.

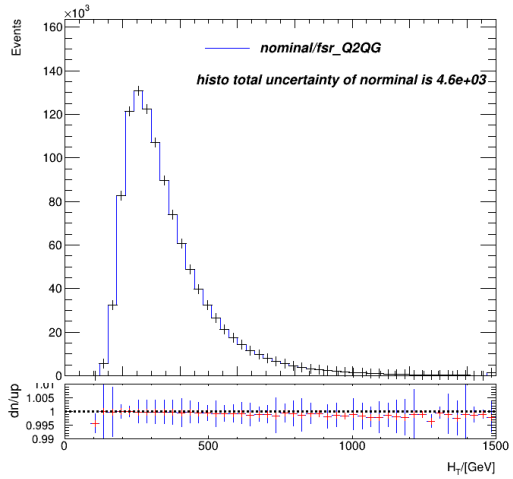

Figure 5.63: H_T distributions with modified error on nominal histograms for the FSR/Q2QG variation in the μ+jet events.

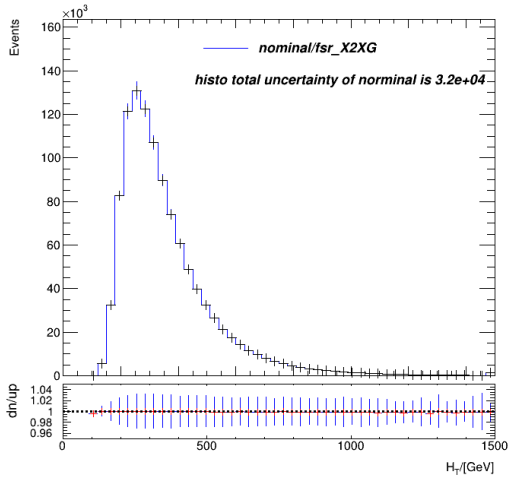

Figure 5.64: H_T distributions with modified error on nominal histograms for the FSR/X2XG variation in the μ+jet events.

Comparing the histogram total uncertainties and error bars in ratio plots, the relation of 4 variations contribution to the uncertainty on nominal histograms could be shown below:

For muon-FSR-H_T: $X2XG > G2GG > G2QQ > Q2QG$

5.3.3 Discussion

The histogram total uncertainty and the maximal relative uncertainty of 4 variations contributing to nominal histograms are summarised in Table 5.3.

Looking at the error bars on histograms and on ratio plots, the impact of 4 variations could be observed and the variations which has the largest uncertainties to nominal histograms and contribute the largest uncertainties to total could be informed.

Comparing the relation of 4 variations contributing uncertainties into total histograms and the relation of 4 variations uncertainties between up and down single lepton: those variations, which have the largest uncertainties between up and down have also the largest uncertainties impact into the total histograms. And those variations which have smallest uncertainty between up and down single lepton have also the smallest uncertainty impact into total histograms.

5.4 Comparison of ISR/FSR uncertainties in the new/old approach with the largest impact variation

In this section, the uncertainties comparison of old and new samples will be processed to see which approach has smaller uncertainty and how much uncertainty has the variation, which has the largest impact, contributed to total histograms.

5.4.1 Explanation

The old samples are plotted nominal histograms with up and down variations and meanwhile the error bars on histograms and ratio plots to show the uncertainties of them.

In ratio plots the ratio between up and down variation is not the main point in comparison, but the error bars on ratio plots, which shows the relative uncertainties of each bin.

In this section, histograms called "total" are produced to summarise 4 variations together to get the whole uncertainties of using new approach.

For total histograms, the bin content are the sum of 4 variations and the error bars for

both histograms and ratio plots are the quadrature summed error from 4 variations. i.e. quadrature sum the difference between 4 variations and nominal histograms, which shows the whole uncertainties influence of 4 variations together on nominal histograms.

5.4.2 Comparison of ISR/FSR uncertainties in the new/old approach with largest impacted variation in e+jet event

Electron-ISR-N_{jets}

Here the comparison of nominal histograms from old and new samples with total uncertainties are processed with also the variation which contributes the largest uncertainties impact into total:

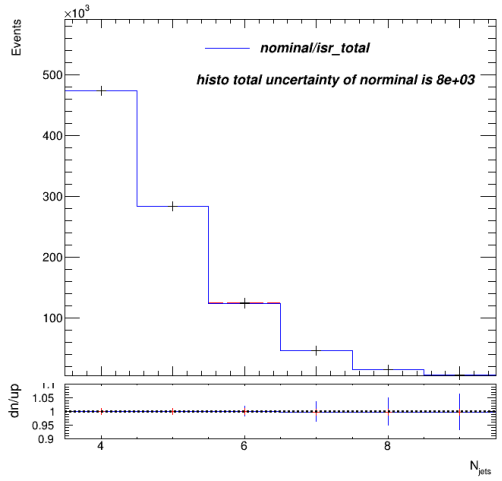

Figure 5.65: Nominal histograms of new samples with total uncertainties.

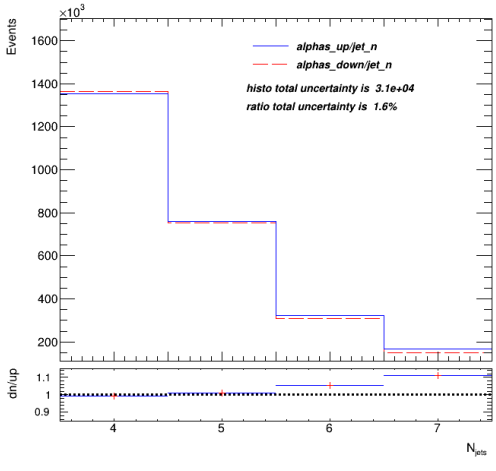

Figure 5.66: Nominal histograms of old samples with total uncertainties.

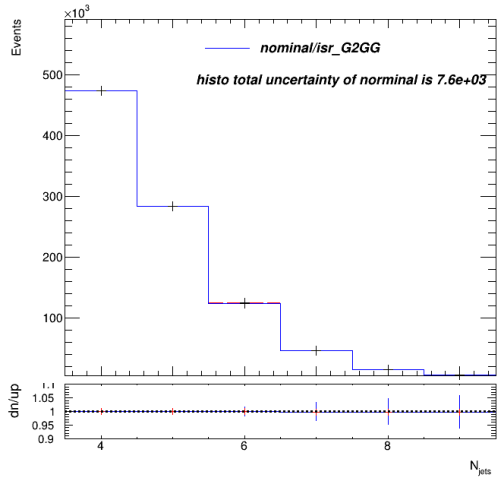

Figure 5.67: G2GG variation has the largest uncertainty impact into total histograms on ISR.

Comparing the total histogram uncertainties of the N_{jets} plots between new samples and old samples and also with G2GG in ISR, new samples have smaller histo total uncertainties and X2XG has contributed around 90% uncertainties of whole.

Electron-ISR-H_T

Here the comparison of nominal histograms from old and new samples with total uncertainties are processed with also the variation which contributes the largest uncertainties impact into total:

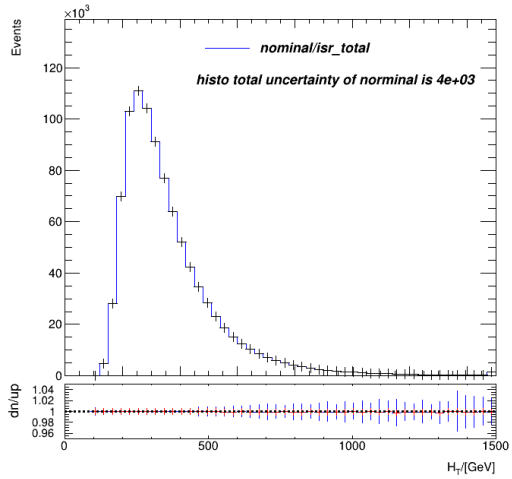

Figure 5.68: Nominal histograms of new samples with total uncertainties.

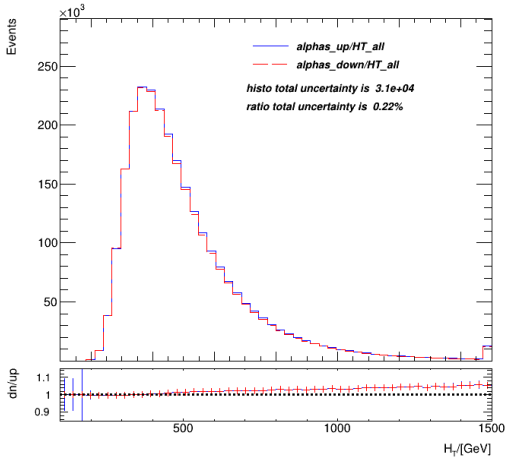

Figure 5.69: Nominal histograms of old samples with total uncertainties.

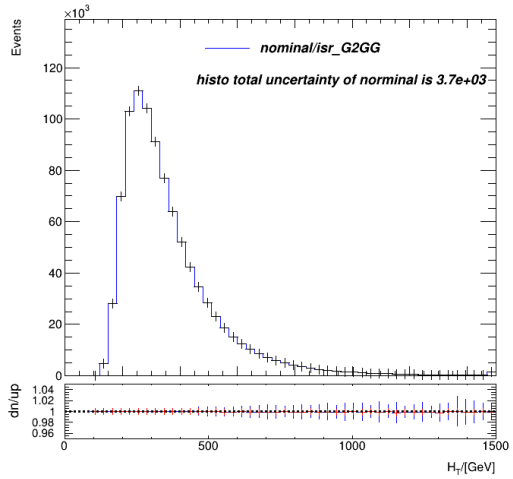

Figure 5.70: G2GG variation has the largest uncertainty impact into total histograms on ISR.

Comparing the total histogram uncertainties of the H_T plots between new samples and old samples and also with G2GG in ISR, new samples have smaller histo total uncertainties and X2XG has contributed around 90% uncertainties of whole.

Electron-FSR-N_{jets}

Here the comparison of nominal histograms from old and new samples with total uncertainties are processed with also the variation which contributes the largest uncertainties impact into total:

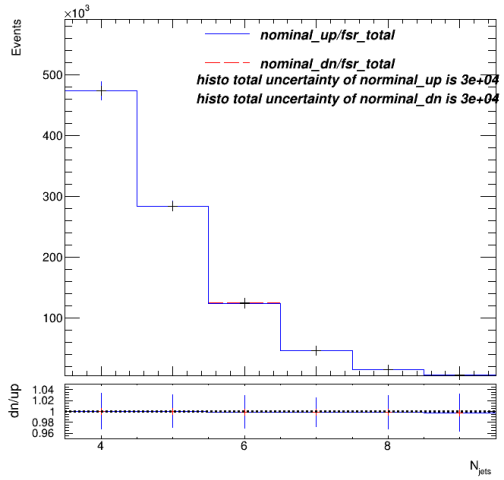

Figure 5.71: Nominal histograms of new samples with total uncertainties.

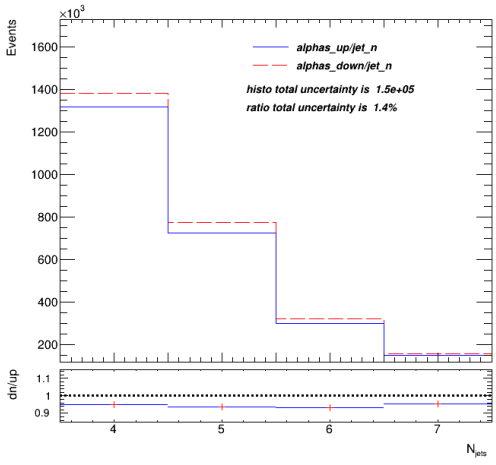

Figure 5.72: Nominal histograms of old samples with total uncertainties.

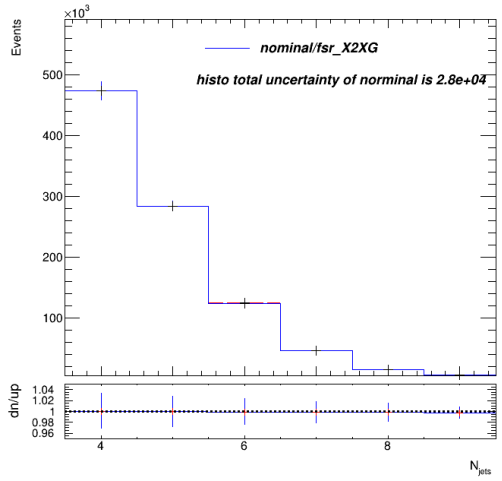

Figure 5.73: X2XG variation has the largest uncertainty impact into total histograms on FSR.

Comparing the total histogram uncertainties of N_{jets} plots between new samples and old samples and also with X2XG in FSR, new samples have smaller histo total uncertainties and X2XG has contributed around 93.3% uncertainties of whole.

Electron-FSR-H_T

Here the comparison of nominal histograms from old and new samples with total uncertainties are processed with also the variation which contributes the largest uncertainties impact into total:

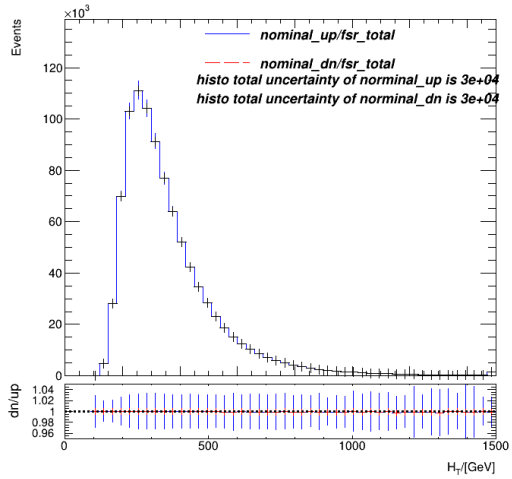

Figure 5.74: Nominal histograms of new samples with total uncertainties.

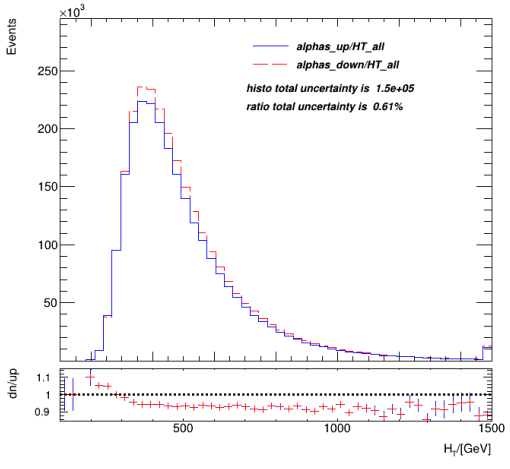

Figure 5.75: Nominal histograms of old samples with total uncertainties.

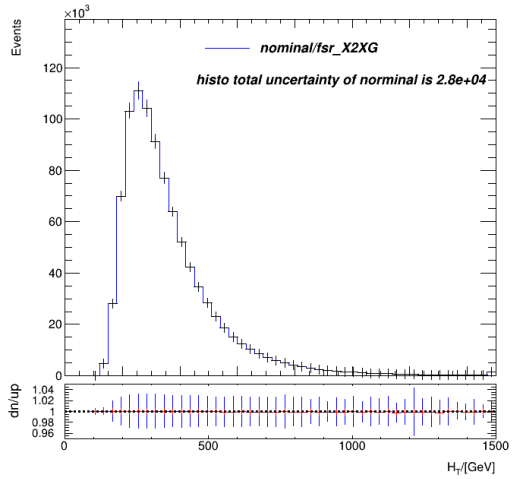

Figure 5.76: X2XG variation has the largest uncertainty impact into total histograms on FSR.

Comparing the total histogram uncertainties of H_T plots between new samples and old samples and also with X2XG in FSR, new samples have smaller histo total uncertainties and X2XG has contributed around 93.3% uncertainties of whole.

5.4.3 Comparison of ISR/FSR uncertainties in the new/old approach with largest impacted variation in μ+jet event

Muon-ISR-N_{jets}

Here the comparison of nominal histograms from old and new samples with total uncertainties are made with also the variation which contributes the largest uncertainties impact into total:

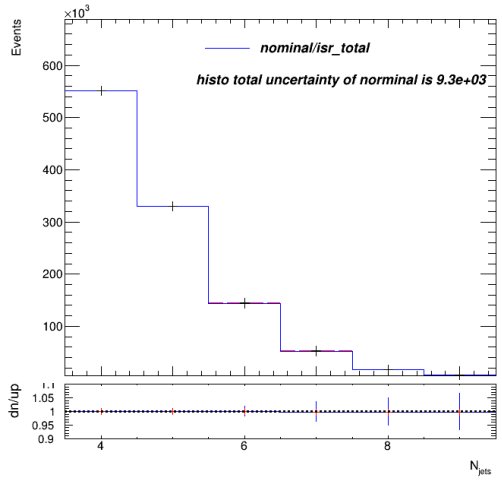

Figure 5.77: Nominal histograms of new samples with total uncertainties.

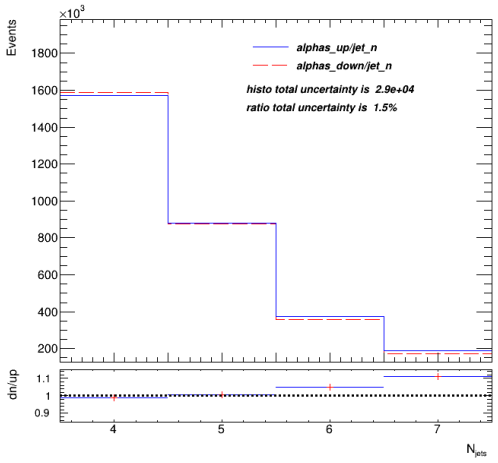

Figure 5.78: Nominal histograms of old samples with total uncertainties.

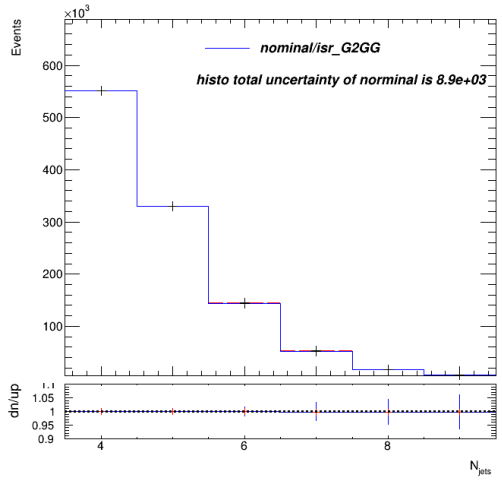

Figure 5.79: G2GG variation has the largest uncertainty impact into total histograms on ISR.

Comparing the total histogram uncertainties of N_{jets} plots between new samples and old samples and also with G2GG in ISR, new samples have smaller histo total uncertainties and G2GG has contributed around 95.7% uncertainties of whole.

Muon-ISR-H_T

Here the comparison of nominal histograms from old and new samples with total uncertainties are processed with also the variation which contributes the largest uncertainties impact into total:

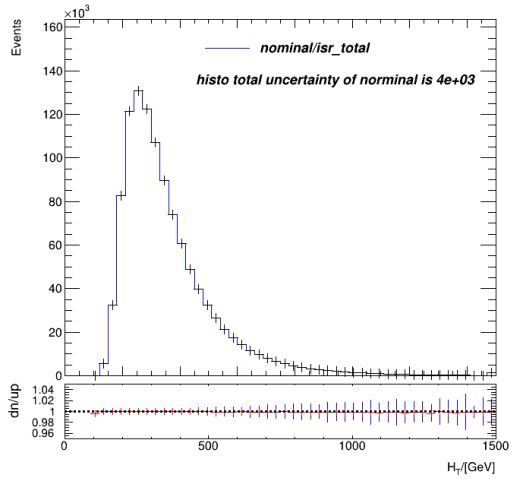

Figure 5.80: Nominal histograms of new samples with total uncertainties.

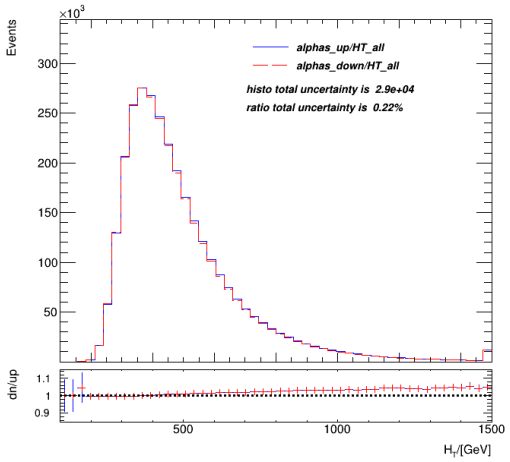

Figure 5.81: Nominal histograms of old samples with total uncertainties.

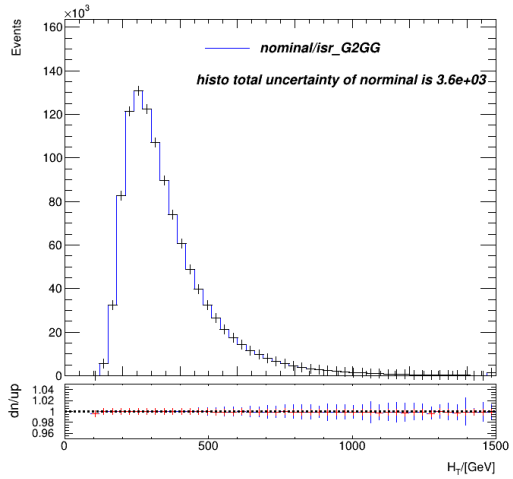

Figure 5.82: G2GG variation has the largest uncertainty impact into total histograms on ISR.

Comparing the total histogram uncertainties of H_T plots between new samples and old samples and also with G2GG in ISR, new samples have smaller histo total uncertainties and G2GG has contributed around 90% uncertainties of whole.

Muon-FSR-N_{jets}

Here the comparison of nominal histograms from old and new samples with total uncertainties are processed with also the variation which contributes the largest uncertainties impact into total:

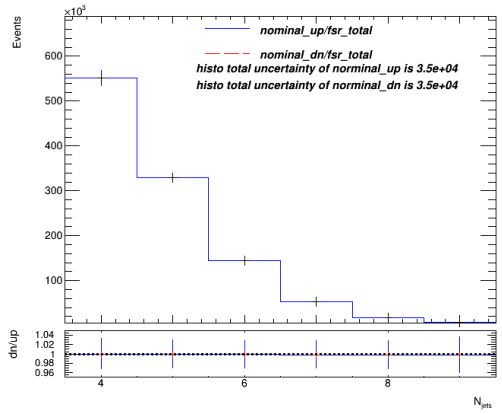

Figure 5.83: Nominal histograms of new samples with total uncertainties.

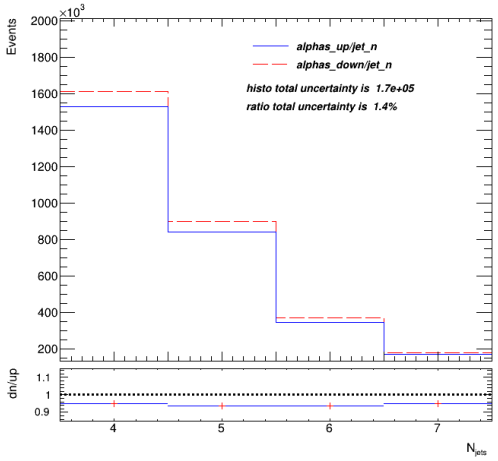

Figure 5.84: Nominal histograms of old samples with total uncertainties.

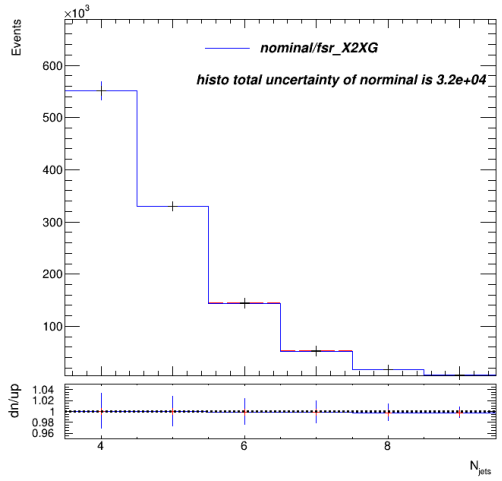

Figure 5.85: X2XG variation has the largest uncertainty impact into total histograms on FSR.

Comparing the total histogram uncertainties of N_{jets} plots between new samples and old samples and also with X2XG in FSR, new samples have smaller histo total uncertainties and X2XG has contributed over 90% uncertainties of whole.

Muon-FSR-H_T

Here the comparison of nominal histograms from old and new samples with total uncertainties are processed with also the variation which contributes the largest uncertainties impact into total:

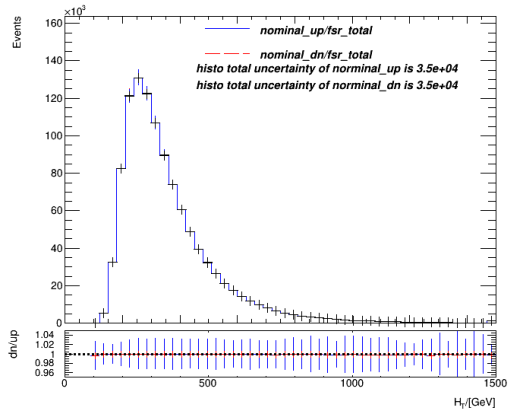

Figure 5.86: Nominal histograms of new samples with total uncertainties.

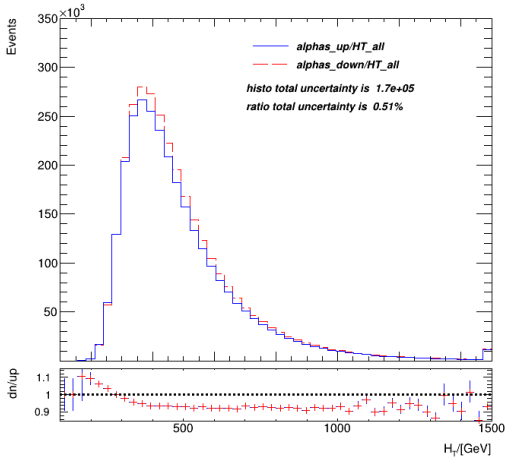

Figure 5.87: Nominal histograms of old samples with total uncertainties.

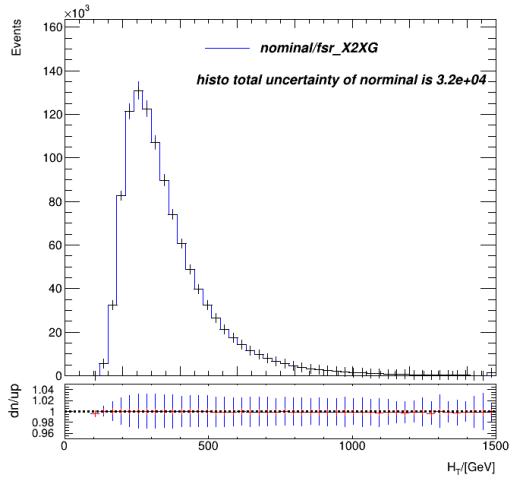

Figure 5.88: X2XG variation has the largest uncertainty impact into total histograms on FSR.

Comparing the total histogram uncertainties of H_T plots between new samples and old samples and also with X2XG in FSR, new samples have smaller histo total uncertainties and X2XG has contributed over 90% uncertainties of whole.

5.4.4 Discussion

The total histogram uncertainties of old and new approach with the largest variation contribution into total histogram are summarised in Table 5.4. Comparing old with new samples: the uncertainties from new approach are smaller than uncertainties from old

approach. And during comparing it is also observed that G2GG variation has contributed the most uncertainties of total uncertainties in ISR and X2XG has contributed the most uncertainties in FSR.

total uncertainty	ISR-G2GG	ISR-G2QQ	ISR-Q2QG	ISR-X2XG	FSR-G2GG	FSR-G2QQ	FSR-Q2QG	FSR-X2XG
e+jet histo	7.4e+03	7.2e+02	2.2e+03	4e+02	1.3e+04	9.3e+03	5.5e+03	5.6e+04
e+jet N_{jets} ratio	1.4%	0.11%	0.56%	0.034%	0.37%	0.69%	0.21%	0.99%
e+jet H_T ratio	0.19%	0.025%	0.14%	0.0082%	0.22%	0.18%	0.11%	0.39%
μ+jet histo	6.8e+03	6.8e+02	2.1e+03	4.3e+02	1.8e+04	1e+04	6.6e+03	6.4e+04
μ+jet N_{jets} ratio	1.4%	0.091%	0.54%	0.033%	0.42%	0.75%	0.2%	0.98%
μ+jet H_T ratio	0.17%	0.021%	0.13%	0.011%	0.28%	0.18%	0.087%	0.38%

Table 5.2: Total histogram uncertainty and total ratio uncertainty of variations of ISR and FSR in e+jet event and μ+jet event.

uncertainty	ISR-G2GG	ISR-G2QQ	ISR-Q2QG	ISR-X2XG	FSR-G2GG	FSR-G2QQ	FSR-Q2QG	FSR-X2XG
e+jet N_{jets} histo	7.6e+03	6.2e+02	2.4e+03	2e+02	6.5e+03	4.7e+03	3.2e+03	2.8e+04
e+jet N_{jets} relative	5%	0.4%	2%	0.2%	0.7%	3%	1%	4%
e+jet H_T histo	3.7e+03	3.7e+02	1.2e+03	2e+02	6.5e+03	4.7e+03	3.9e+03	2.8e+04
e+jet H_T relative	3%	0.5%	2%	0.1%	5%	3%	1%	4%
μ+jet N_{jets} histo	8.9e+03	6.6e+02	2.7e+03	2.2e+02	9.1e+03	5.1e+03	3.7e+03	3.2e+04
μ+jet N_{jets} relative	7%	0.5%	2%	0.2%	1%	4%	1%	4%
μ+jet H_T histo	3.6e+03	3.7e+02	1.3e+03	2.2e+02	9e+03	5.1e+03	4.6e+03	3.2e+04
μ+jet H_T relative	3%	0.2%	2%	0.2%	1%	3%	1%	4%

Table 5.3: Total histogram uncertainty and relative uncertainty of variations of ISR and FSR in e+jet event and μ+jet event.

	old	new	largest variation
e+jet-ISR-N_{jets}	3.1e+04	8e+03	7.6e+03
e+jet-ISR-H_T	3.1e+04	4e+03	3.6+03
e+jet-FSR–N_{jets}	1.5e+05	3e+04	2.8e+04
e+jet-FSR–H_T	1.5e+05	3e+04	2.8e+04
μ+jet-ISR-N_{jets}	2.9e+04	9.3e+03	8.9e+03
μ+jet-ISR-H_T	2.9e+04	4e+03	3.6e+03
μ+jet-FSR-N_{jets}	1.7e+05	3.5e+04	3.2e+04
μ+jet-FSR-H_T	1.7e+05	3.5e+04	3.2e+04

Table 5.4: Comparison of total histogram uncertainties from old and new approach with largest impact variation.

6 Conclusion and outlook

6.1 Summary

6.1.1 On total uncertainty level

Comparing the total uncertainty generated by the new and old approaches which are introduced in section **??**, it was found that using the new approach can significantly reduce the total uncertainty and the total uncertainty generated by the new approach in a single lepton channel is about only 20% of the old approach. In the new approach, the variable, which is introduced in Table 4.1, with the most uncertainty contributes more than 90% of the total uncertainty. In ISR, the variable with the most uncertainty is G2GG, and in FSR it is X2XG.

What also to pay attention to is the relative uncertainty of 4 variation impact on total histograms. For the ISR variation, the relative uncertainty of N_{jets} plots and H_T plots for G2GG is all over 3% and reaches 7% sometime and for Q2QG is all over 2%. On the contrary, the relative uncertainty for G2QQ are under 0.5% and especially for X2XG under 0.2%.

For the FSR variation, the situation is completely reversed. For both, G2QQ and X2XG, the relative uncertainties are above 3% and for G2GG and Q2QG, the relative uncertainties are under 1%. But there is one exception in particular, the H_T plot for FSR/G2GG has the maximum relative uncertainty around 5% at 1400 GeV. Out of this peak the relative uncertainties of the remaining bins are under 2%, which is relatively small.

6.1.2 On 4 variations level

Comparing the 4 variations in the new approach, the difference of the uncertainty between "up" and "down" variation also causes the large uncertainty which finally leads to the total uncertainty.

For the ISR variation, G2GG and Q2QG have large histogram uncertainties and ratio

uncertainties and G2QQ and X2XG have small uncertainties, which is consistent with their performance on the total uncertainties.
For the FSR variation, X2XG and G2QQ have large uncertainties while Q2QG has small uncertainties, which is also consistent with their performance in the total uncertainties. The exception here is also the G2GG variation, which has sometimes the second largest histograms in both N_{jets} and H_T plots and for ratio uncertainties the second in H_T plots and the third in N_{jets} plots. The main reason for that is the large uncertainty at around 1400 GeV.

6.1.3 On "up" and "down" variation level

In general, the single electron channel and the single muon channel do not show much difference, so it is reasonable to combine them into single lepton channel. Looking at N_{jets} and H_T plots of 4 variations in both ISR and FSR variations in single lepton channel, some observalous can also be summarized.
For N_{jets} plots, the difference between up and down in ratio plots has increased with increasing N. Exception here is FSR/G2GG and FSR/X2XG. The difference between up and down in ratio plots is, that for FSR/G2GG the uncertainties first increase and reach a maximum 3% at N=6 and afterwards decrease and for FSR/X2XG has largest difference around 6% at N=4, and after that constantly decrease to 2% at N=9.
For H_T plots, the difference between up and down in the ratio plots normally increases as the transverse momentum increases and for G2GG and G2QQ variation, there is always a peak at around 1400 GeV, which increases total ratio uncertainties. The exception here is FSR/Q2QG and FSR/X2XG. The difference between up and down in ratio plots for FSR/Q2QG has a decrease from 4% at around 125 GeV to 1% at 200 GeV at the beginning, and for FSR/X2XG the uncertainties has increased extremely rapidly to 6% at 200 GeV. Therefore, for transverse momentum under 200 GeV in the FSR variation, Q2QG has contributed the largest uncertainty among 4 variations and above 200 GeV, X2XG has contributed the most uncertainty. The physical explaintion for this observation is, at low momentum, i.e. transverse momentum under 200 GeV, the uncertainties of analysis mainly come from one quark (in this analysis means up, down, charm or strange quark) splitting into same type quark and gluon and for momentum above 200 GeV, the uncertainties mainly comes from other types of particles (in this analysis means bottom or top quark) splitting into same type particle and gluon.

6.2 Outlook

By analysing the relation of uncertainties from 4 variations contributed into total histograms and also the uncertainties of up and down variation for 4 variations in the new approach has been summarised in section 6.1. But during the analysis there are also some problems remaining which need to be studied deeply to understand the cause of the large uncertainty.

Comparing the histogram total uncertainties in the N_{jets} and H_T plots of 4 variations in different state radiation (ISR and FSR) in the new approach from Table 5.2 and Table 5.3, it could be observed that not only the uncertainties between "up" and 'down" variation of 4 variations in single lepton+jets events but also the uncertainties of 4 variations in nominal histograms, FSR has always larger impact on the $t\bar{t}$ systematic model in analysis than ISR.

To explore the reason of the large uncertainty contribution in the FSR variation, it is necessary to dig further about which impact the large uncertainty on the total uncertainty in the new approach. The main problem which needs to be investigated further is the large uncertainty around 1400 GeV in the H_T plots, which causes the large uncertainties in G2GG and G2QQ variations in the FSR variation. Deeply understanding this problem may lead to a solution why FSR has larger uncertainties on the $t\bar{t}$ systematic model in $t\bar{t}$ cross section analysis than the ISR one.

Another problem which needs to be considered is the large uncertainties at low H_T values. In the new approach, the selection of momentum is above 25 GeV. During making the plots, some bins at low H_T values have bin content of 0, which would cause trouble by calculating the ratio total uncertainty if they are not selected out, and they always have larger uncertainties comparing to bins above 200 GeV. This is shown in comparison plots of "up" and "down" variations in both new approach and old approach. By reasonably increasing the selection standard, the total ratio uncertainties could rapidly decrease without the bins which cause large uncertainties and the analysis may become more meaningful and accurate.

It would be necessary to study the impact of the new uncertainties in the signal regions of the $t\bar{t}$ single lepton+jets cross-section measurement. This includes not only the variation of the three fit variables, but also the impact of the uncertainties in the profile likelihood fit that is used to extract the cross-section and its uncertainties.

Bibliography

[1] S. Abachi, et al. (DØ), *Observation of the top quark*, Phys. Rev. Lett. **74**, 2632 (1995)

[2] F. Abe, et al. (CDF), *Observation of top quark production in $\bar{p}p$ collisions*, Phys. Rev. Lett. **74**, 2626 (1995)

[3] M. Tanabashi, et al. (Particle Data Group), *Review of Particle Physics*, Phys. Rev. **D98(3)**, 030001 (2018)

[4] M. Czakon, P. Fiedler, A. Mitov, *Total Top-Quark Pair-Production Cross Section at Hadron Colliders Through $O(\hat{\mathrm{I}} \pm \frac{4}{S})$*, Phys. Rev. Lett. **110**, 252004 (2013)

[5] *Measurement of the $t\bar{t}$ production cross-section in the lepton+jets channel at $\sqrt{s} = 13$ TeV with the ATLAS experiment*, Technical Report ATLAS-CONF-2019-044, CERN, Geneva (2019)

[6] G. Aad, et al. (ATLAS), *The ATLAS Experiment at the CERN Large Hadron Collider*, JINST **3**, S08003 (2008)

[7] S. Mrenna, P. Skands, *Automated Parton-Shower Variations in Pythia 8*, Phys. Rev. **D94(7)**, 074005 (2016)

Acknowledgements

First of all, I want to thank my parents. Without their unselfish emotional and financial support, I cannot successfully complete my thesis, especially during the virus pandemic. I also want to thank my girlfriend for taking care of me and helping to deal with daily matters when I am busy at work.

Secondly, I would like to thank many people who supported me in my work. First, I want to express my sincere thanks to Dr. Thomas Peiffer, who has given me inestimable help and support from the beginning to the end, from software support, the plan, the specific algorithm to the final modification work. I can't solve many problems and complete this paper without his help. Secondly, I would like to express my sincere gratitude to Marcel Niemeyer and Prof. Dr. Baida Achkar, who gave me meticulous help to guide me to finally solve all kinds of problems encountered. In the early stage of work, Marcel Niemeyer guided me meticulously and patiently at work and answered many of my very basic questions, and also helped me organize the code to make it more readable and standardized. Later in the work, Professor Baida was very patient and meticulous and gave me a lot of help and clarified the next goal. At the same time, she also provided me with a lot of information and codes to help me better understand and carry out my work. Of course, I also want to express my gratitude to Ishan Pokharel, Fabian Sohns, Dr. Tomas Dado and Dr. Elizaveta Shabalina, who have helped me in my work and answered and pointed out many questions.

Finally, I want to express my sincere thanks to Prof. Dr. Arnulf Quadt and the University of Göttingen for giving me the opportunity to study in depth. It not only enriched my knowledge but also deepened my interest and desire for further exploration in the field of particle physics.

Erklärung nach §13(9) der Prüfungsordnung für den Bachelor-Studiengang Physik und den Master-Studiengang Physik an der Universität Göttingen:
Hiermit erkläre ich, dass ich diese Abschlussarbeit selbständig verfasst habe, keine anderen als die angegebenen Quellen und Hilfsmittel benutzt habe und alle Stellen, die wörtlich oder sinngemäß aus veröffentlichten Schriften entnommen wurden, als solche kenntlich gemacht habe.
Darüberhinaus erkläre ich, dass diese Abschlussarbeit nicht, auch nicht auszugsweise, im Rahmen einer nichtbestandenen Prüfung an dieser oder einer anderen Hochschule eingereicht wurde.

Göttingen, den 30. Juli 2020

(Jun Huang)